Electronic Supplementary Information

Steric modulation of *o*-carborane enables tunable single and dual emission in multi-resonance TADF compounds

Young Hoon Lee,[a†] Rafi Muhammad Lutfi,[a†] Junseong Lee,[b] Eunsung Lee,[c] Jaehoon Jung*[a] and Min Hyung Lee*[a]

[a] Department of Chemistry, University of Ulsan, Ulsan 44610, Republic of Korea

[b] Department of Chemistry, Chonnam National University, Gwangju 61186, Republic of Korea

[c] Department of Chemistry, Seoul National University, Seoul 08826, Republic of Korea

Table of Contents

General considerations····· S2
Synthesis····· S2
X-ray crystallography····· S5
Cyclic voltammetry····· S6
Photophysical measurements····· S6
Theoretical calculations····· S6
NMR Spectra····· S8
TGA curves····· S14
Crystal packing····· S14
Cyclic voltammograms····· S15
Photophysical properties····· S16
Computational details····· S19
References····· S31

General considerations

All operations were performed under an inert nitrogen atmosphere using standard Schlenk and glove box techniques. Anhydrous grade solvents (Aldrich) were dried over activated molecular sieves (5Å). Spectrophotometric-grade toluene and tetrahydrofuran (THF) were used as received from Aldrich and Alfa, respectively. Commercial reagents were used without further purification after purchase. Compounds **1a**[1] and DtBuCzB (**5**)[2] were synthesized according to the modified literature procedures. Deuterated solvents from Eurisotop were used. NMR spectra were recorded on a Bruker AVANCE III HD 400 (400.13 MHz for ^{1}H, 100.61 MHz for ^{13}C, 128.38 MHz for ^{11}B) spectrometer at ambient temperature. Chemical shifts are given in ppm, and are referenced against external Me_4Si (^{1}H, ^{13}C) and $BF_3{\cdot}OEt_2$ (^{11}B). Elemental analyses were performed on a Flash 2000 elemental analyzer (Thermo Scientific). Thermogravimetric analysis (TGA) was performed with a TA Instruments Q50 under an N_2 atmosphere at a heating rate of 10 °C/min. Cyclic voltammetry experiments were carried out using a CHI600E system.

Synthesis

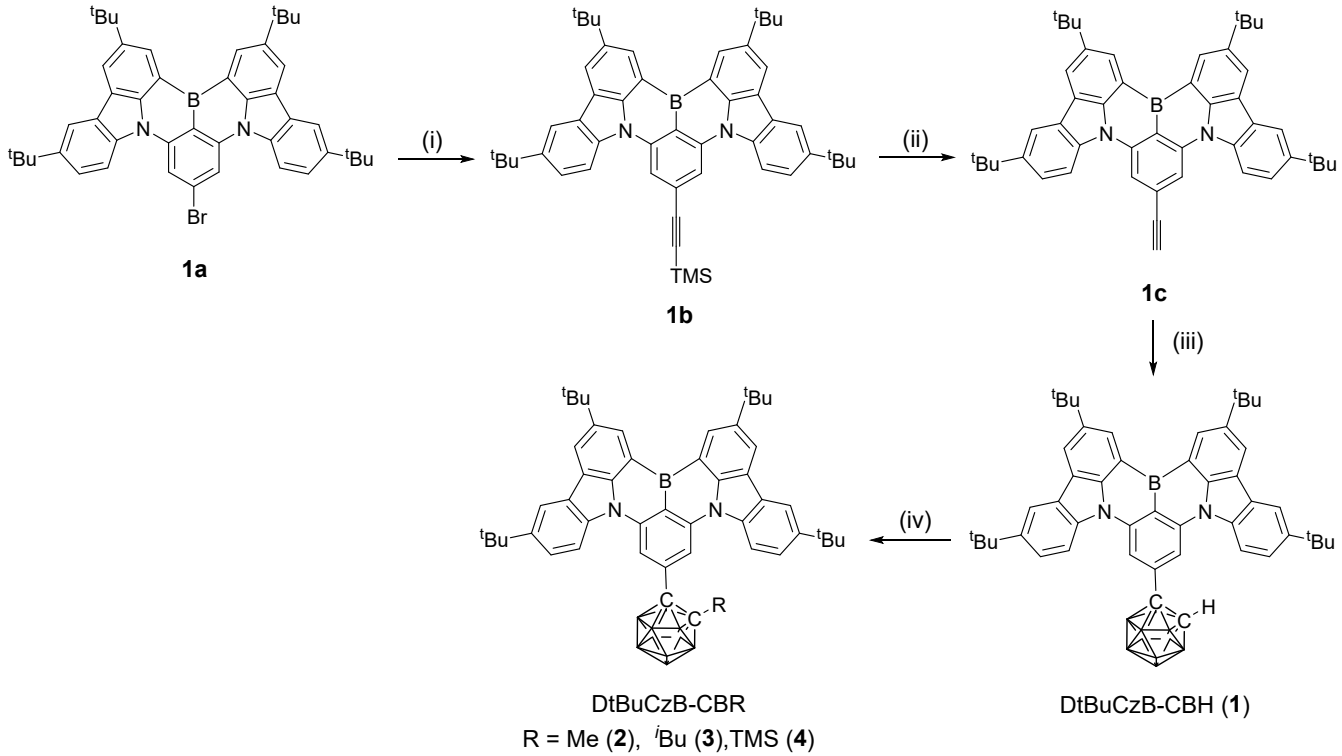

Scheme S1. Synthetic procedures of DtBuCzB-CBR (R = H (**1**), Me (**2**), ^{i}Bu (**3**), TMS (**4**)): (i) ethynyltrimethylsilane, $Pd(PPh_3)_4$, CuI, Et_3N, toluene, 50 °C, 5 h. (ii) K_2CO_3, CH_2Cl_2/MeOH (2:1), RT, overnight. (iii) $B_{10}H_{14}$, Et_2S, toluene, reflux, 3 d. (iv) LDA, diethyl ether or THF, −30 °C, 1 h then MeI (for **2**), $SiMe_3Cl$ (for **3**), and ^{i}BuI (for **4**), −30 °C, RT, 1 h.

Synthesis of 1b

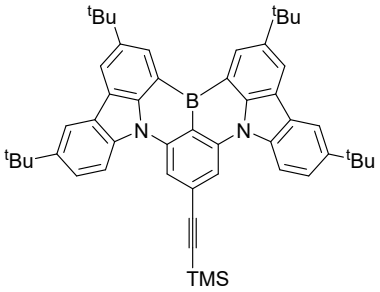

A mixture of **1a** (0.47 g, 0.14 mmol), ethynyltrimethylsilane (0.3 mL, 2.11 mmol), $Pd(PPh_3)_4$ (25 mg, 0.022 mmol), and CuI (10 mg, 0.053 mmol) in NEt_3/toluene (30 mL, 1:2, v/v) was stirred at 50 °C for 5 h. After cooling down to room temperature, the solvent was evaporated under reduced pressure and purified by column chromatography on silica gel using CH_2Cl_2/*n*-hexane (1:7, v/v) as eluent. The eluate was concentrated under reduced pressure and recrystallized in CH_2Cl_2/MeOH to afford **1b** as a yellow powder (Yield: 0.38 g, 79%). ^{1}H NMR (400.13 MHz, $CDCl_3$, 298 K): δ 9.12 (sd, J = 1.6 Hz, 2H, Ar*H*), 8.47–8.40 (m, 6H, Ar*H*), 8.26 (sd, J = 2.0 Hz, 2H, Ar*H*), 7.73 (dd, J = 8.8, 2.0 Hz, 2H, Ar*H*), 1.69 (s, 18H, −C(CH_3)$_3$), 1.56 (s, 18H, −C(CH_3)$_3$), 0.43 (s, 9H, −Si(CH_3)$_3$). ^{13}C{^{1}H} NMR (100.61 MHz, $CDCl_3$, 298 K): δ 145.4, 144.7, 143.9, 141.5, 138.1, 129.7, 127.3, 127.0, 124.5, 123.66, 120.8, 117.2, 114.2, 111.1, 105.8, 96.3, 35.2, 34.8, 32.2, 31.8, 0.11.

Synthesis of 1c

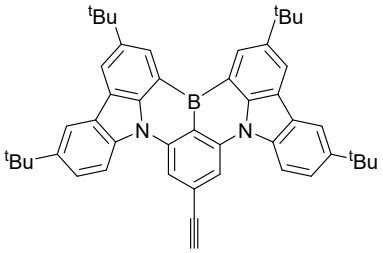

A mixture of **1b** (0.52 g, 0.71 mmol) and K_2CO_3 (0.4 g, 2.89 mmol) in CH_2Cl_2/MeOH (30 mL, 2:1, v/v) was stirred at room temperature overnight. The solvent was evaporated under reduced pressure and the resulting solid was extracted with diethyl ether. The combined organic layer was dried over $MgSO_4$, filtered, and purified by column chromatography on silica gel using CH_2Cl_2/*n*-hexane (1:3, v/v) as eluent. The eluate was concentrated under reduced pressure and recrystallized in CH_2Cl_2/MeOH to afford **1c** as a yellow powder (Yield: 0.47 g, 98%). ^{1}H NMR (400.13 MHz, $CDCl_3$, 298 K): δ 9.11 (sd, J = 1.6 Hz, 2H, Ar*H*), 8.47 (sd, J = 1.6 Hz, 2H, Ar*H*), 8.41 (s, 2H, Ar*H*), 8.38 (d, J = 9.2 Hz, 2H, Ar*H*), 8.26 (sd, J = 2.0 Hz, 2H, Ar*H*), 7.69 (dd, J = 8.8, 2.0 Hz, 2H, Ar*H*), 3.38 (s, 1H, −C≡C*H*), 1.69 (s, 18H, −C(CH_3)$_3$), 1.56 (s, 18H, −C(CH_3)$_3$). ^{13}C{^{1}H} NMR (100.61 MHz, $CDCl_3$, 298 K): δ 145.5, 144.8, 144.0, 141.5, 138.1, 129.8, 127.0, 126.2, 124.5, 123.7, 120.9, 117.2, 114.1, 111.2, 84.5, 78.8, 35.2, 34.8, 32.2, 31.8. Anal. Calcd (%) for $C_{48}H_{49}BN_2$: C, 86.73; H, 7.43; N, 4.21. Found: C, 86.81; H, 7.37; N, 4.23.

Synthesis of 1

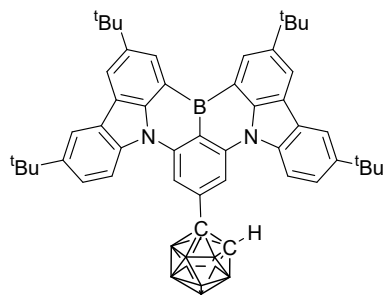

A mixture of **1c** (0.47 g, 0.71 mmol), $B_{10}H_{14}$ (0.1 g, 0.82 mmol), and Et_2S (0.4 mL, 3.71 mmol) in toluene (20 mL) was refluxed for 3 days

under nitrogen atmosphere. After cooling down to room temperature, the resulting solution was concentrated under reduced pressure and purified by column chromatography on silica gel using CH_2Cl_2/*n*-hexane (1:7, v/v) as eluent. The eluate was concentrated under reduced pressure and recrystallized in CH_2Cl_2/MeOH to afford **1** as an orange-yellow powder (Yield: 0.46 g, 82%). ^{1}H NMR (400.13 MHz, $CDCl_3$, 298 K): δ 9.10 (sd, J = 1.6 Hz, 2H, Ar*H*), 8.50 (sd, J = 2.0 Hz, 2H, Ar*H*), 8.44 (s, 2H, Ar*H*), 8.31–8.28 (m, 4H, Ar*H*), 7.79 (dd, J = 8.8, 2.0 Hz, 2H, Ar*H*), 4.21 (s, 1H, −CB*H*), 1.69 (s, 18H, −C(CH_3)$_3$), 1.58 (s, 18H, −C(CH_3)$_3$). ^{13}C{^{1}H} NMR (100.61 MHz, CD_2Cl_2, 298 K): δ 146.1, 145.0, 143.9, 141.5, 137.7, 136.9, 129.5, 127.1, 125.0, 123.7, 121.5, 117.8, 114.1, 107.5, 77.3, 61.8, 35.1, 34.8, 31.8, 31.6. ^{11}B{^{1}H} NMR (128.38 MHz, CD_2Cl_2, 298 K): δ 44.3 (–*B*Ar$_3$), −1.2, −2.4, −8.6, −9.7, −11.0 (–$B_{10}H_{11}$). Anal. Calcd (%) for $C_{48}H_{59}B_{11}N_2$: C, 73.64; H, 7.60; N, 3.58. Found: C, 73.68; H, 7.58; N, 3.54. T_{d5} = 399 °C.

Synthesis of 2

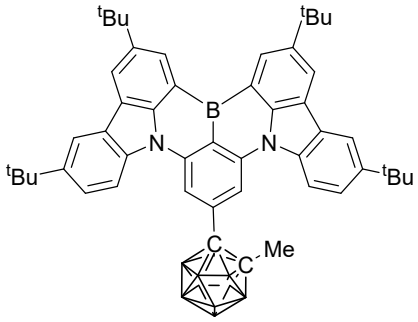

To a solution of **1** (0.1 g, 0.13 mmol) in THF (15 mL) was added dropwise lithium diisopropylamide (LDA, 2 M in THF, 0.1 mL, 0.20 mmol) at −30 °C. The mixture was stirred at −30 °C for 1 h and then MeI (0.04 mL, 0.64 mmol) was added at −30 °C. After stirring at room temperature for 1 h, distilled water (50 mL) was added and extracted with CH_2Cl_2 (20 mL × 3). The combined organic layer was dried over Mg_SO_4, filtered, and, purified by column chromatography on silica gel using CH_2Cl_2/*n*-hexane (1:20, v/v) to afford **2** as a yellow powder (Yield: 0.082g, 80%). Single crystals suitable for X-ray diffraction analysis were obtained by slow evaporation of a mixed CH_2Cl_2/MeOH solution of **2**. ^{1}H NMR (400.13 MHz, $CDCl_3$, 298 K): δ 9.14 (sd, J = 1.6 Hz, 2H, Ar*H*), 8.61 (s, 2H, Ar*H*), 8.56 (sd, J = 1.6 Hz, 2H, Ar*H*), 8.36–8.33 (m, 4H, Ar*H*), 7.80 (dd, J = 8.8, 2.0 Hz, 2H, Ar*H*), 1.92 (s, 3H, −CBCH_3), 1.67 (s, 18H, −C(CH_3)$_3$), 1.54 (s, 18H, −C(CH_3)$_3$). ^{13}C{^{1}H} NMR (100.61 MHz, $CDCl_3$, 298 K): δ 146.1, 145.4, 144.2, 141.7, 138.0, 135.2, 129.9, 127.3, 125.1, 124.0, 121.6, 121.3, 117.6, 113.7, 110.4, 82.8, 78.0, 35.3, 34.9, 32.2, 31.8, 23.5. ^{11}B{^{1}H} NMR (128.38 MHz, $CDCl_3$, 298 K): δ 49.2 (–*B*Ar$_3$), −3.7, −4.9, −9.7 (–$B_{10}H_{10}$). Anal. Calcd (%) for $C_{49}H_{61}B_{11}N_2$: C, 73.85; H, 7.72; N, 3.52. Found: C, 73.90; H, 7.68; N, 3.56. T_{d5} = 413 °C.

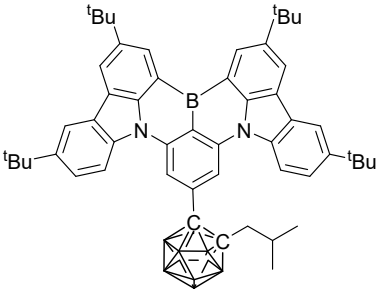

Synthesis of 3

This compound was prepared in a manner analogous to the synthesis of **2** using **1** (0.12 g, 0.15 mmol), LDA (0.15 mL, 0.30 mmol), and ^{i}BuI

(0.04 mL, 0.35 mmol) in THF (20 mL), affording **3** as a yellow powder (Yield: 0.06 g, 48%). ^{1}H NMR (400.13 MHz, $CDCl_3$, 298 K): δ 9.18 (sd, J = 2.0 Hz, 2H, Ar*H*), 8.64 (s, 2H, Ar*H*), 8.62 (sd, J = 2.0 Hz, 2H, Ar*H*), 8.41 (sd, J = 2.0 Hz, 2H, Ar*H*), 8.38 (d, J = 8.8 Hz, 2H, Ar*H*), 7.87 (dd, J = 8.8, 2.0 Hz, 2H, Ar*H*), 1.98 (d, J = 5.6 Hz, 2H, −CH_2−), 1.90 (septet, 6.4 Hz, 1H, −C*H*(CH_3)$_2$), 1.73 (s, 18H, −C(CH_3)$_3$), 1.62 (s, 18H, −C(CH_3)$_3$), 0.83 (d, J = 6.8 Hz, 6H, −CH(CH_3)$_2$). ^{13}C{^{1}H} NMR (100.61 MHz, CD_2Cl_2, 298 K): δ 146.3, 145.5, 144.2, 141.6, 138.0, 135.1, 129.9, 127.2, 125.2, 124.0, 121.6, 117.8, 113.7, 110.6, 85.0, 83.6, 43.9, 35.2, 34.8, 31.9, 31.6, 29.7, 28.6, 23.1. ^{11}B{^{1}H} NMR (128.38 MHz, CD_2Cl_2, 298 K): δ 43.5 (–*B*Ar$_3$), −3.7, −10.1 (–$B_{10}H_{10}$). Anal. Calcd (%) for $C_{52}H_{67}B_{11}N_2$: C, 74.44; H, 8.05; N, 3.34. Found: C, 74.48; H, 7.97; N, 3.40. T_{d5} = 366 °C.

Synthesis of 4

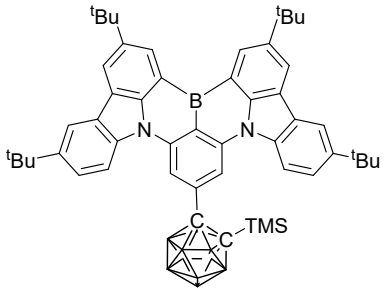

This compound was prepared in a manner analogous to the synthesis of **2** using **1** (0.2 g, 0.26 mmol), LDA (0.13 mL, 0.26 mmol), and $SiMe_3Cl$ (0.04 mL, 0.32 mmol) in diethyl ether (30 mL) affording **4** as a yellow powder (Yield: 0.14 g, 62%). Single crystals suitable for X-ray diffraction analysis were obtained by slow evaporation of a mixed CH_2Cl_2/MeOH solution of **4**. ^{1}H NMR (400.13MHz, $CDCl_3$, 298 K): δ 9.15 (sd, J = 1.6 Hz, 2H, Ar*H*), 8.65 (s, 2H, Ar*H*), 8.52 (sd, J = 1.6 Hz, 2H, Ar*H*), 8.37 (d, J = 8.8 Hz, 2H, Ar*H*), 8.32 (sd, J = 1.6 Hz, 2H, Ar*H*), 7.82 (dd, J = 8.8, 2.0 Hz, 2H, Ar*H*), 1.69 (s, 18H, −C(CH_3)$_3$), 1.58 (s, 18H, −C(CH_3)$_3$), 0.02 (s, 9H, −Si(CH_3)$_3$). ^{13}C{^{1}H} NMR (100.61 MHz, CD_2Cl_2, 298 K): δ 146.6, 145.5, 144.0, 141.6, 138.0, 137.1, 129.9, 127.2, 125.2, 123.9, 121.5, 117.8, 113.6, 110.7, 83.9, 77.5, 35.1, 34.8, 31.9, 31.5, −0.4. ^{11}B{^{1}H} NMR (128.38 MHz, CD_2Cl_2, 298 K): δ 44.6 (–*B*Ar$_3$), 1.7, 0.9, −1.3, −2.4, −8.3, −9.6, −10.9 (–$B_{10}H_{10}$). Anal. Calcd (%) for $C_{51}H_{67}B_{11}N_2Si$: C, 71.64; H, 7.90; N, 3.28. Found: C, 71.61; H, 7.93; N, 3.21. T_{d5} = 376 °C.

X-ray crystallography

Single crystals of suitable size and quality of DtBuCzB-CBMe (**2**) and DtBuCzB-CBTMS (**4**) were coated with Paratone oil and mounted onto a glass capillary. Diffraction data were obtained at 150 K. The crystallographic measurements were performed on a Bruker Apex II CCD area detector diffractometer with graphite-monochromated Mo-Kα radiation (λ = 0.71073 Å). The structures were solved by direct methods and refined by applying full-matrix least-squares fitting on F^2 using SHELXL program package[3] and Olex2.[4] All non-hydrogen atoms were refined with anisotropic displacement parameters. Full details of the structure determinations have been deposited as cifs with the Cambridge Crystallographic Data

Collection under CCDC deposition numbers 2462988 (**2**) and 2462989 (**4**). These data can be obtained free of charge via www.ccdc.cam.ac.uk/data_request/cif.

Cyclic voltammetry

Cyclic voltammetry measurements were carried out in CH_2Cl_2 (1×10^{-3} M) for oxidation using a three-electrode cell configuration consisting of platinum working and counter electrodes and a $Ag/AgNO_3$ (0.01 M in CH_3CN) reference electrode at room temperature. Tetra-*n*-butylammonium hexafluorophosphate (0.1 M) was used as the supporting electrolyte. The oxidation potentials were recorded at a scan rate of 100 mV/s and were reported with reference to the ferrocene/ferrocenium (Fc/Fc^+) redox couple. The HOMO energy levels were determined from the electrochemical oxidation ($E_{1/2}$) peaks of cyclic voltammograms while the LUMO energy levels were estimated from the optical bandgap (E_g) and the HOMO levels.

Photophysical measurements

UV/Vis absorption and photoluminescence (PL) spectra were recorded on a UV-2600 (Shimadzu) and an Edinburgh Instruments FLS1000 spectrophotometer, respectively. Dilute sample solutions (typically 20 μM in oxygen-free solvent) were prepared in a glove box at ambient conditions. Photoluminescence quantum yields (PLQYs) of all the film and solution samples were measured on an absolute PL quantum yield spectrophotometer (Quantaurus-QY C11347-11, Hamamatsu Photonics) equipped with a 3.3-inch integrating sphere. Transient PL decays were measured on an FLS1000 spectrophotometer with an excitation light source of EPL-375 laser for prompt fluorescence and Xenon flashlamp for delayed fluorescence. The photophysical analysis done by using FLS1000 and Quantaurus-QY C11347-11 spectrophotometers was conducted at total-period analysis center for Ulsan chemical industry of KBSI.

Theoretical calculations

Density functional theory (DFT) and time-dependent DFT (TDDFT) calculations were performed to investigate the ground and excited states of compounds **1**–**5**. TDDFT calculations employed the Tamm-Dancoff approximation (TDA).[5] The ground (S_0) states of compounds were optimized using DFT calculations, and their lowest singlet (S_1) and two triplet (T_1 and T_2) excited states were optimized using TDDFT calculations utilizing the PBE0 hybrid functional[6] and the def2-SVP[7] basis set implemented in GAUSSIAN 16 software package.[8] The influence of a different solvent medium (toluene and THF) on the geometric and electronic structures was examined using the polarizable continuum model (PCM) within a self-consistent reaction field (SCRF) approximation.[9] Natural transition orbital (NTO)[10] analysis

was conducted to characterize the excited states of compounds using the Multiwfn program.[11] The compositions of frontier molecular orbitals (FMOs) were computed using the AOMix program.[12] The spin-orbit coupling matrix elements (SOCME) values were evaluated using the quasi-degenerate perturbation theory,[13] implemented in the ORCA software package,[14] with the same functional and basis set as those used in the DFT and TDDFT calculations.

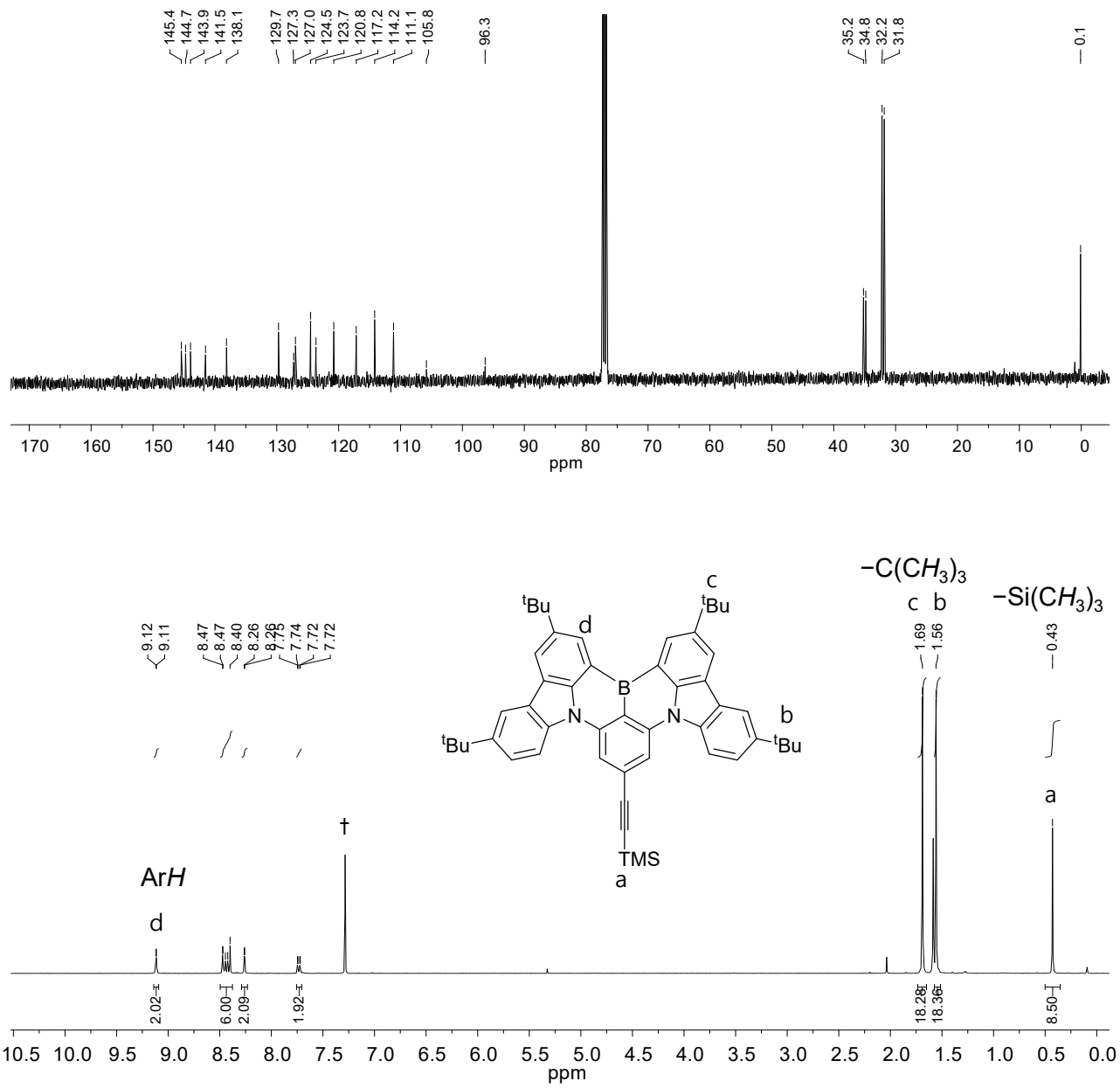

Fig. S1. $^{13}C\{^{1}H\}$ (top) and ^{1}H (bottom) NMR spectra of **1b** in $CDCl_3$ at 298 K († from $CHCl_3$).

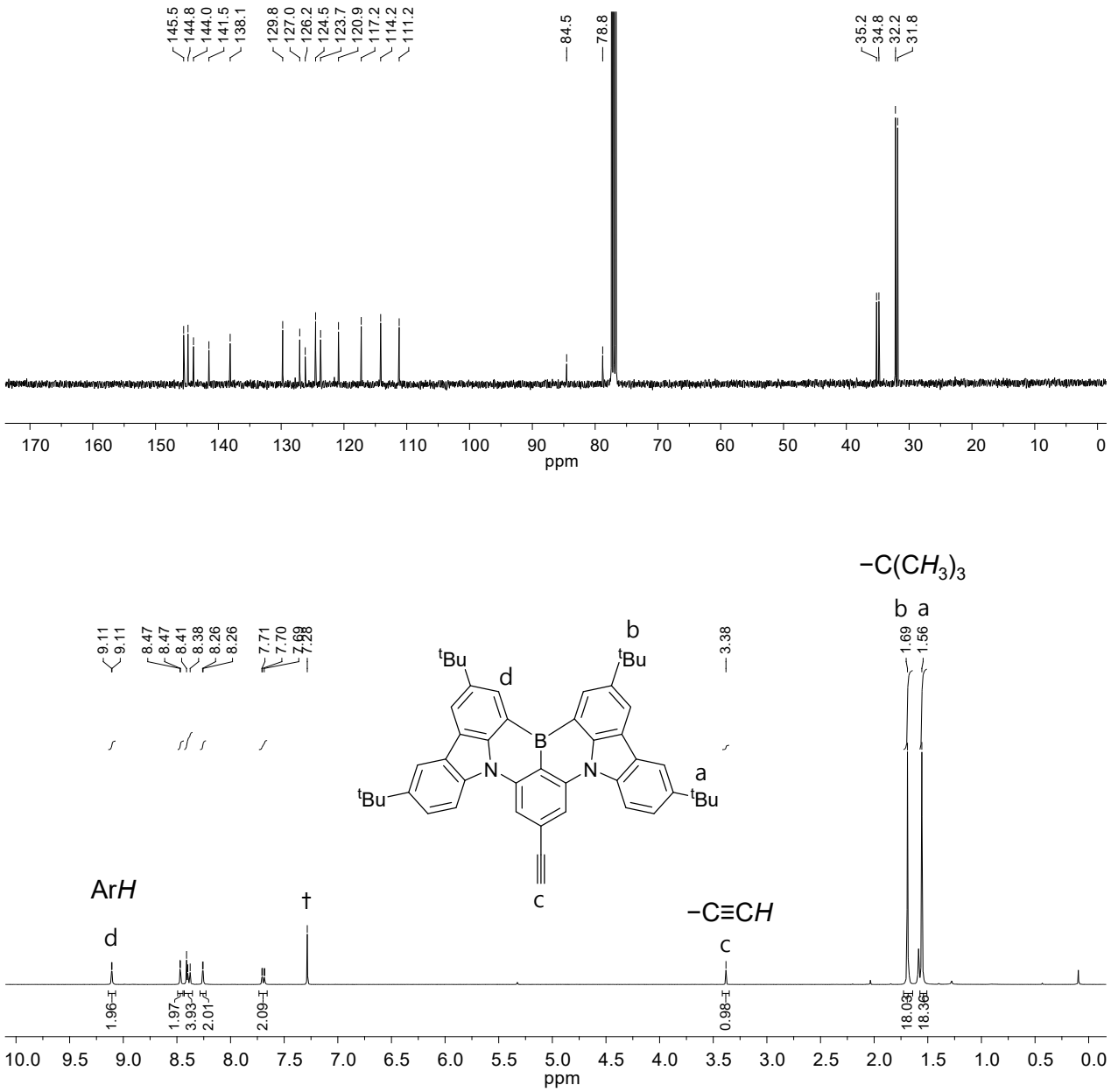

Fig. S2. $^{13}C\{^{1}H\}$ (top) and ^{1}H (bottom) NMR spectra of **1c** in $CDCl_3$ at 298 K († from $CHCl_3$).

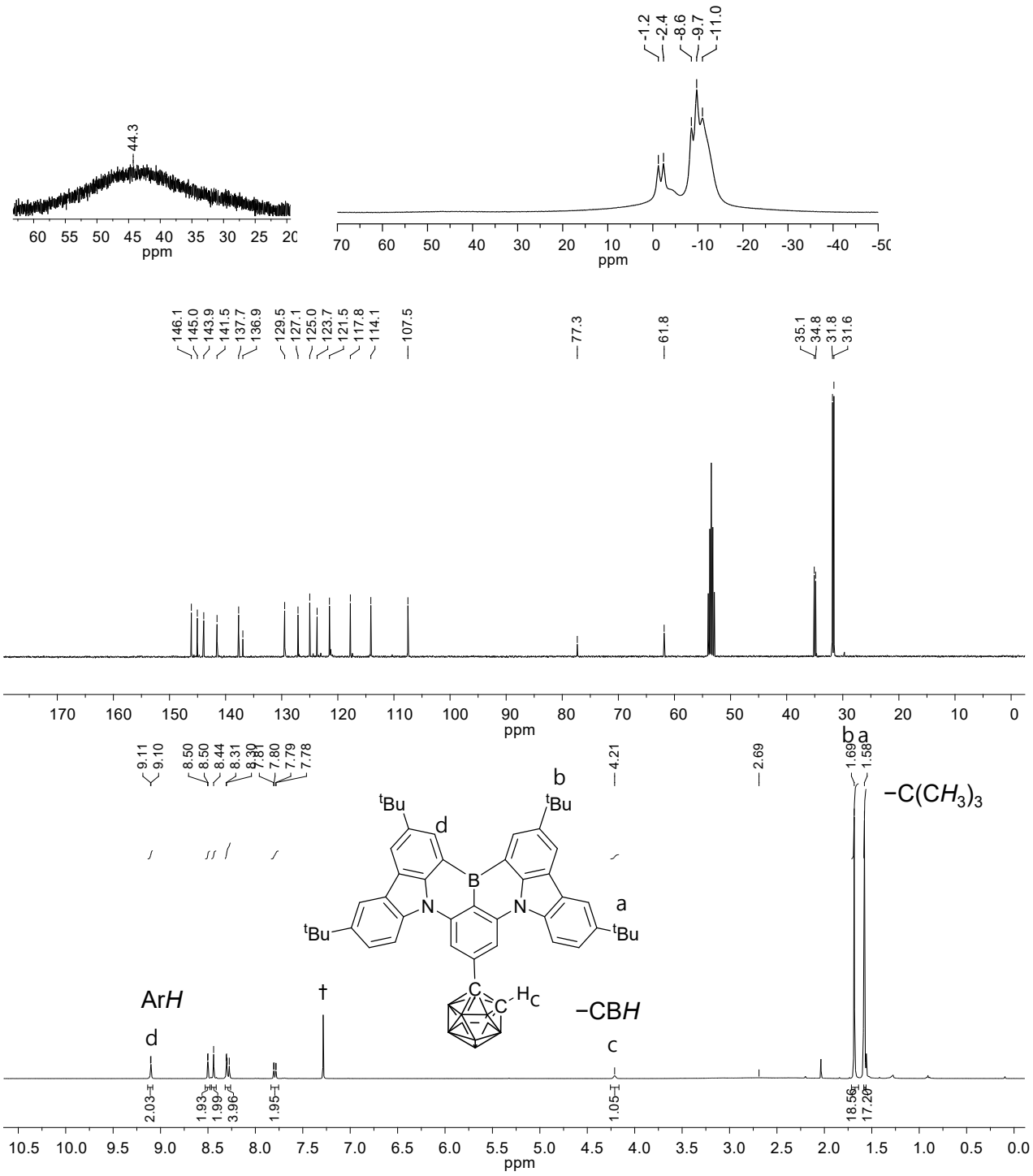

Fig. S3. $^{11}B\{^1H\}$ (top), $^{13}C\{^1H\}$ (middle), and ^1H (bottom) NMR spectra of **1** in $CDCl_3$ at 298 K († from $CHCl_3$).

.

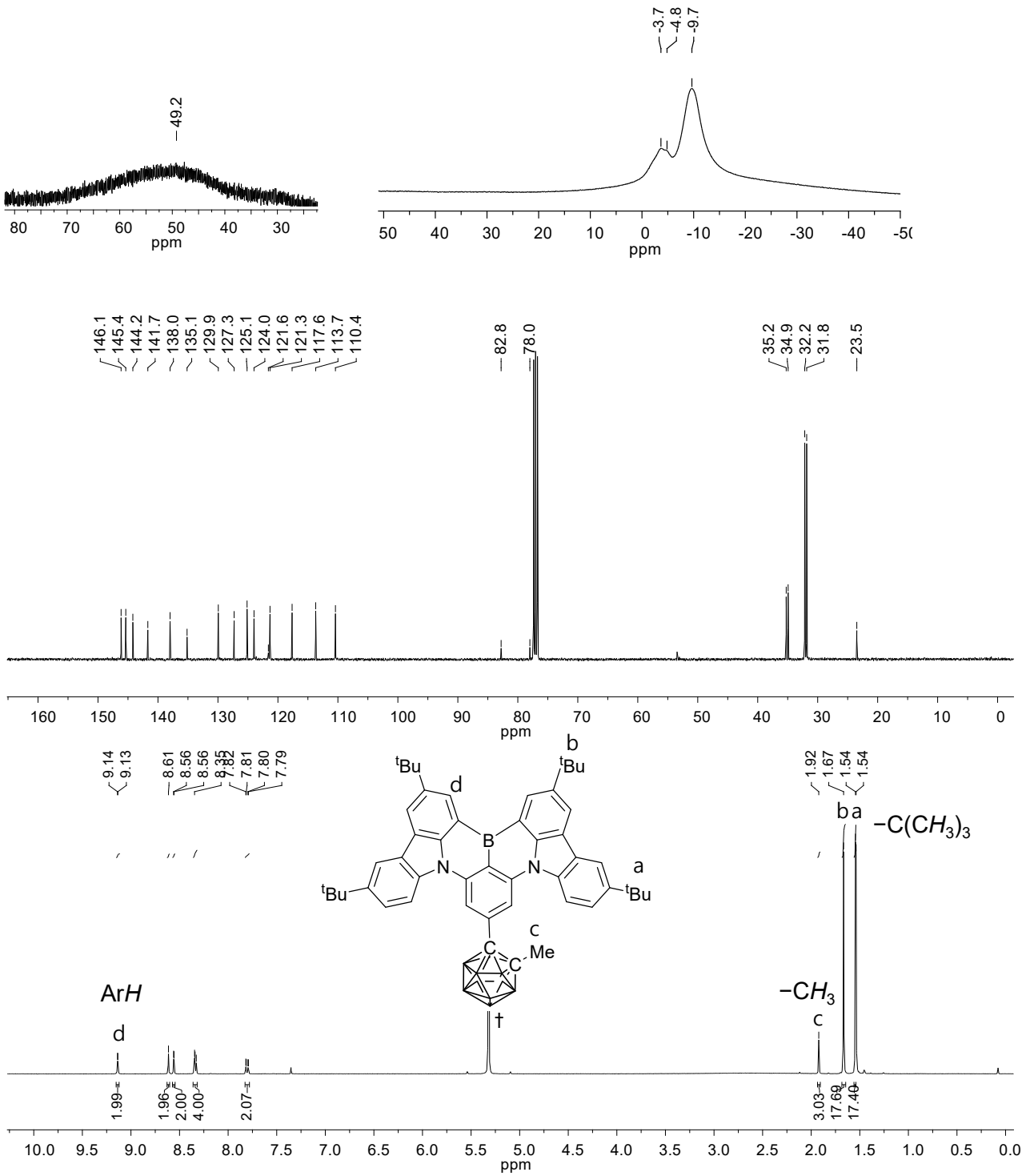

Fig. S4. $^{11}B\{^1H\}$ (top), $^{13}C\{^1H\}$ (middle), and ^1H (bottom) NMR spectra of **2** in CD_2Cl_2 at 298 K († from $CDHCl_2$).

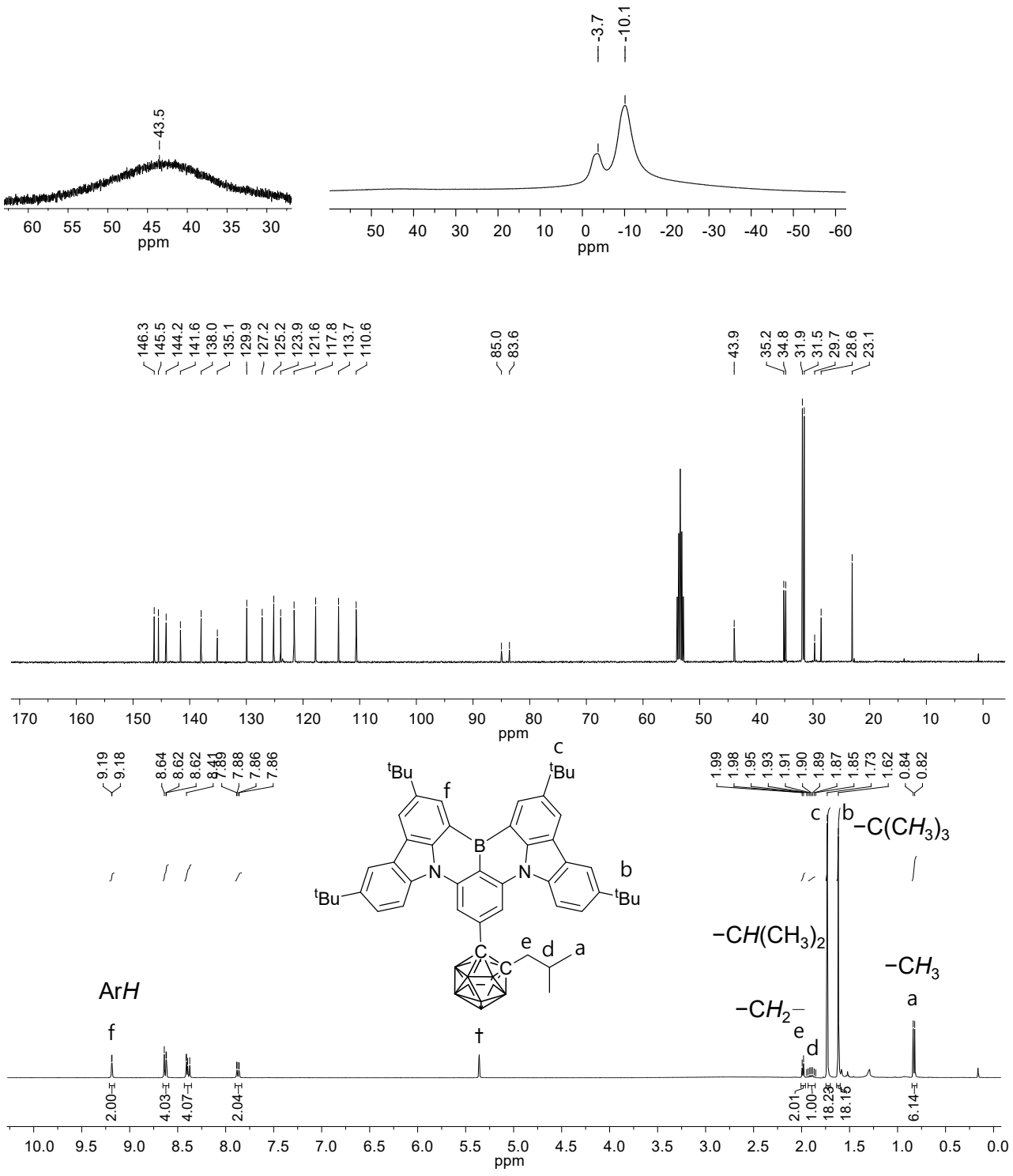

Fig. S5. $^{11}B\{^1H\}$ (top), $^{13}C\{^1H\}$ (middle), and ^1H (bottom) NMR spectra of **3** in CD_2Cl_2 at 298 K († from $CDHCl_2$).

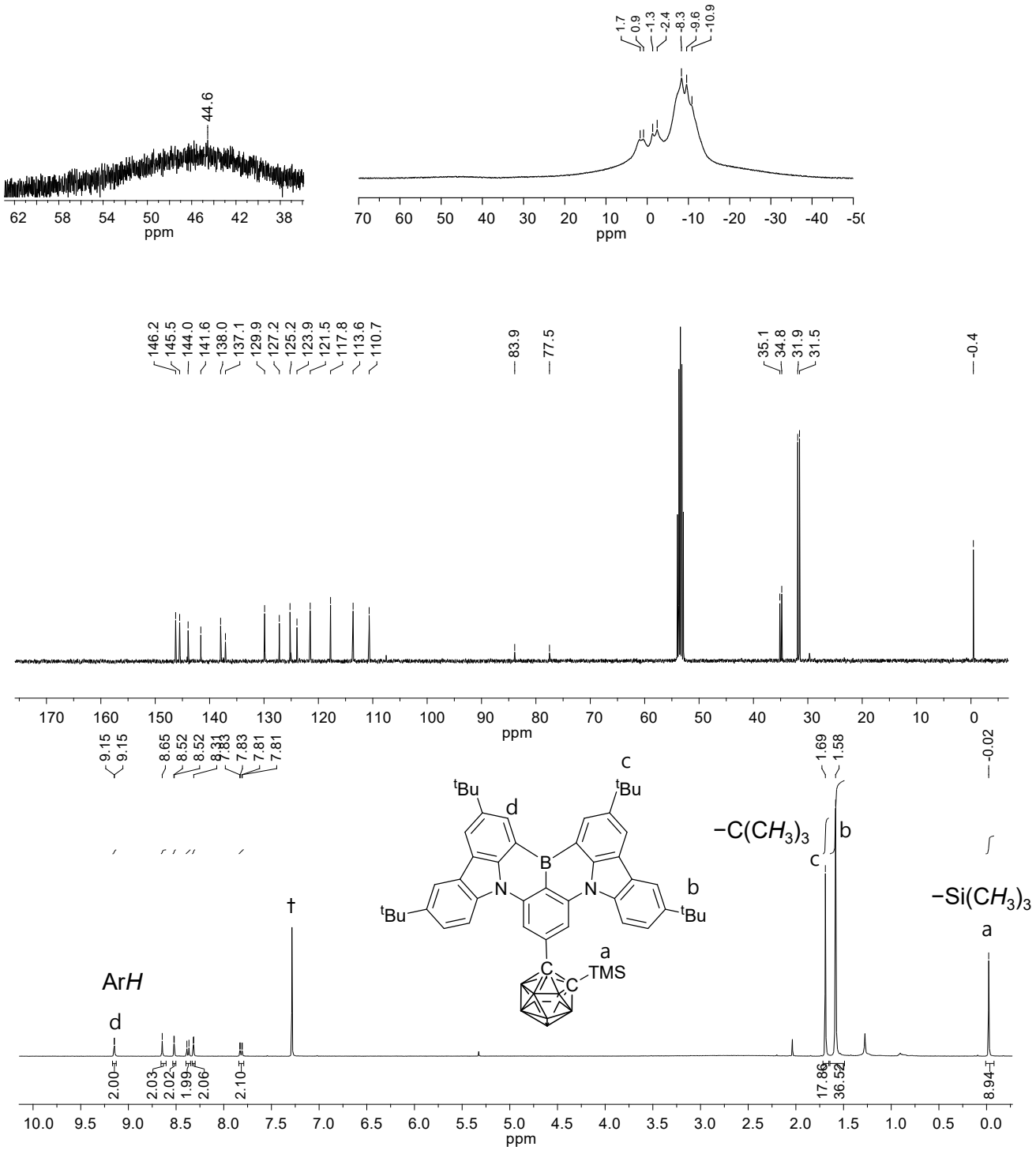

Fig. S6. $^{11}B\{^1H\}$ (top), $^{13}C\{^1H\}$ (middle), and ^1H (bottom) NMR spectra of **4** in CD_2Cl_2 at 298 K († from $CDHCl_2$).

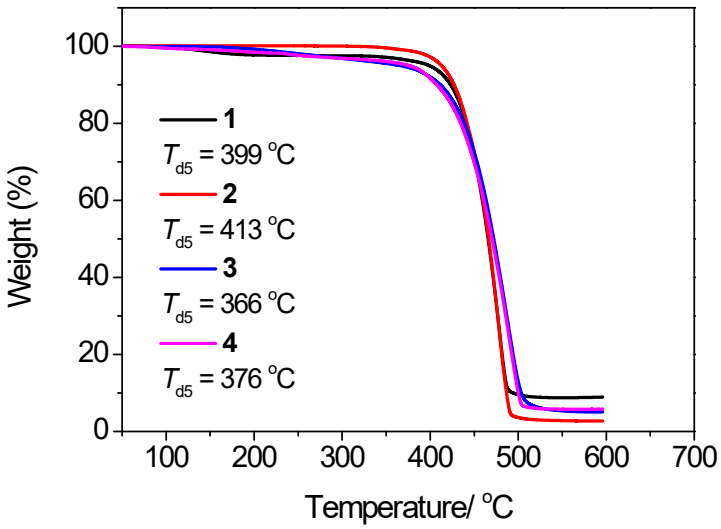

Fig. S7. TGA curves of **1**–**4**.

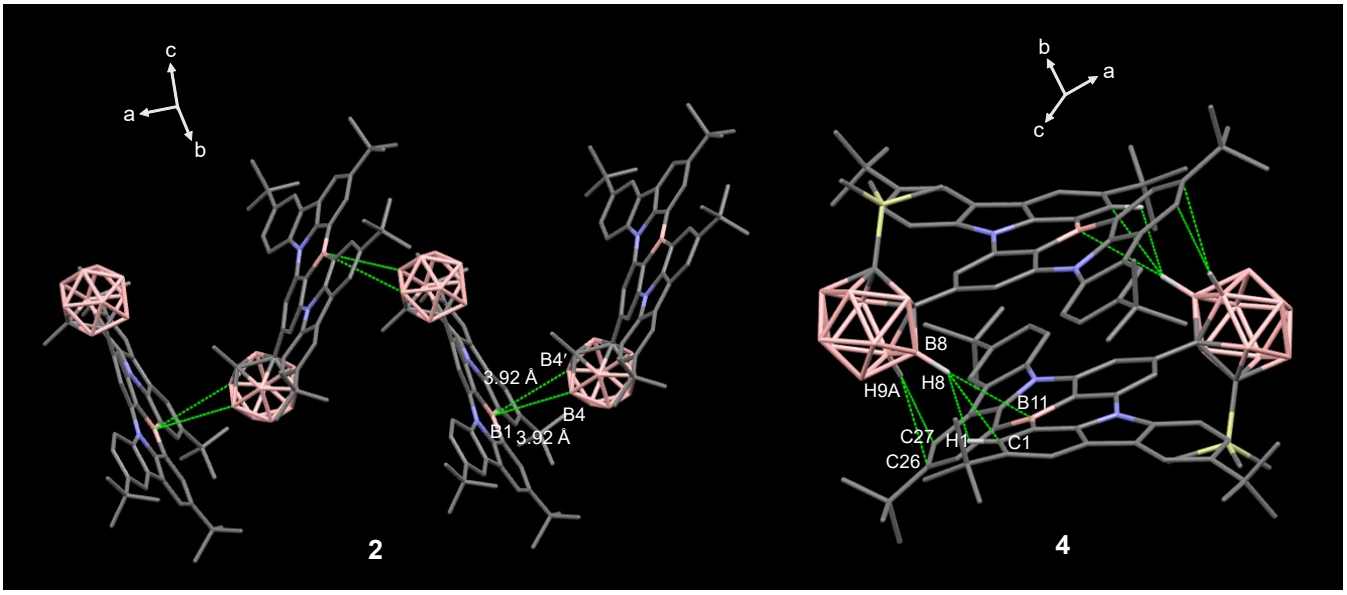

Fig. S8. Crystal packing of **2** and **4** showing short contacts (green dotted line). B4(B4′)···B1 = 3.920 Å for **2** and B9–H9A···C27 = 2.843 Å, B9–H9A···C26 = 2.884 Å, B8–H8···B11 = 3.047 Å, B8–H8···C1 = 2.868 Å, and B8–H8···H1–C1 = 2.353 Å for **4**. C (gray), N (blue), pink (B), and H (white), respectively.

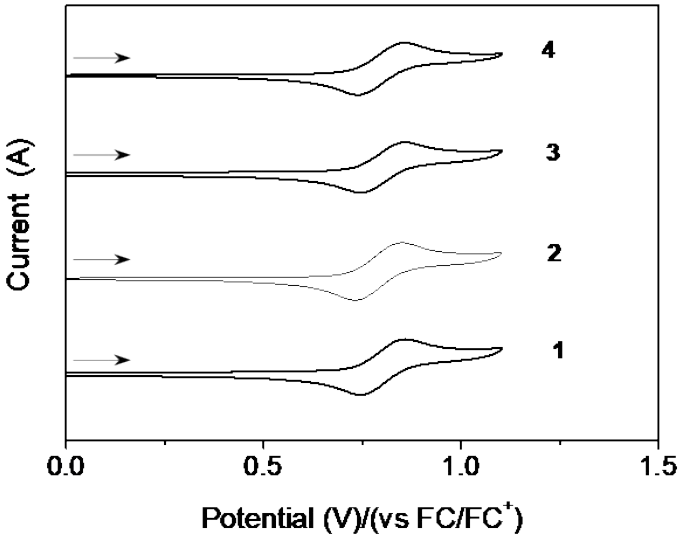

DtBuCzB-CBR	E_g (eV)[a]	E_{ox} (V)[b]	E_{HOMO} (eV)	E_{LUMO} (eV)
1 (H)	2.55	0.78	−5.58	−3.03
2 (Me)	2.54	0.79	−5.59	−3.05
3 (^{t}Bu)	2.54	0.80	−5.60	−3.06
4 (TMS)	2.54	0.80	−5.60	−3.06
5[c]	2.55		−5.40	−2.85

[a] Optical bandgap from the absorption onset wavelength. [b] Half potential ($E_{1/2}$). [c] Data from ref. 2.

Fig. S9. Cyclic voltammograms of **1**–**4** showing oxidation (1.0×10^{-3} M in CH_2Cl_2, scan rate = 100 mV/s).

Photophysical properties

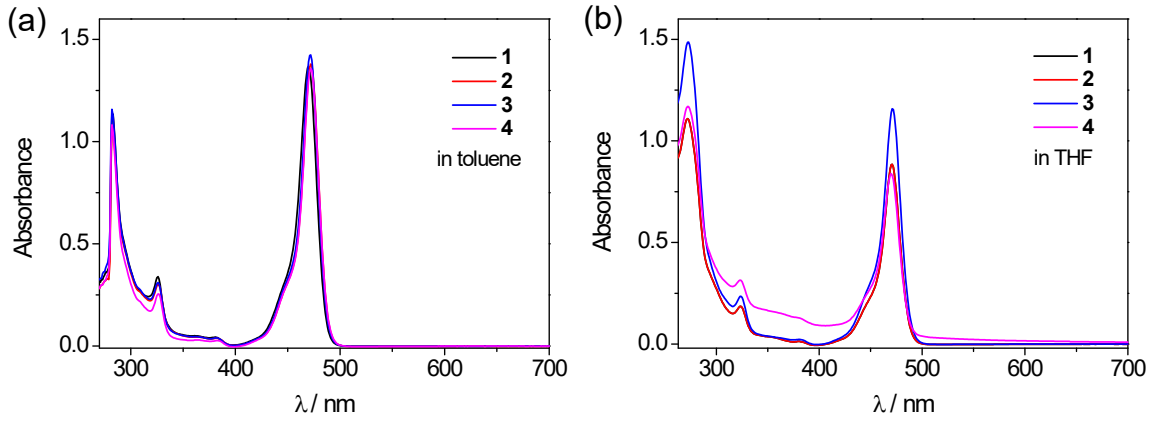

Fig. S10. Absorption spectra of **1**−**4** (a) in toluene and (b) in THF at 298 K (2.0×10^{-5} M).

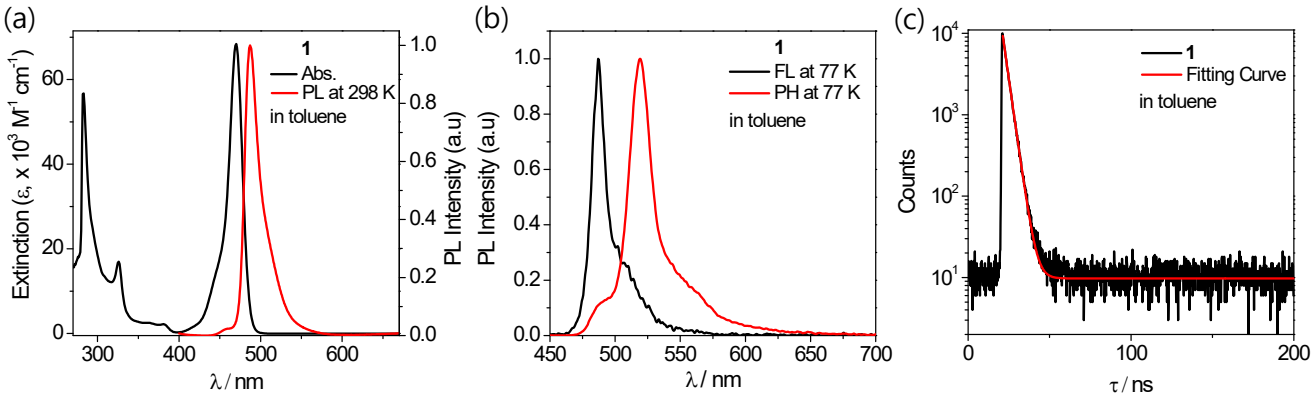

Fig. S11. (a) UV/Vis absorption and PL spectra at 298 K, (b) fluorescence and phosphorescence spectra at 77 K, and (c) transient PL decay curve of **1** at 298 K (2.0×10^{-5} M in toluene).

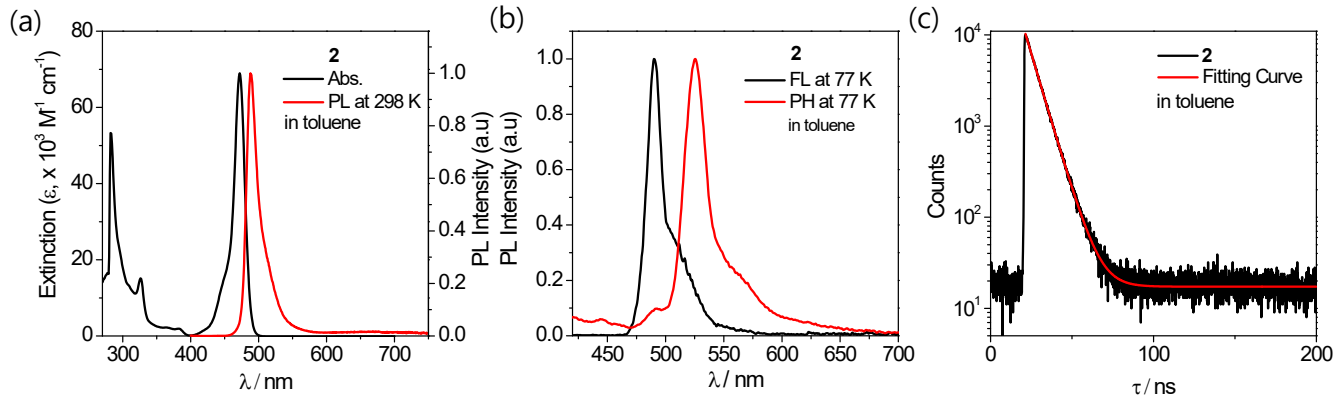

Fig. S12. (a) UV/Vis absorption and PL spectra at 298 K, (b) fluorescence and phosphorescence spectra at 77 K, and (c) transient PL decay curve of **2** at 298 K (2.0×10^{-5} M in toluene).

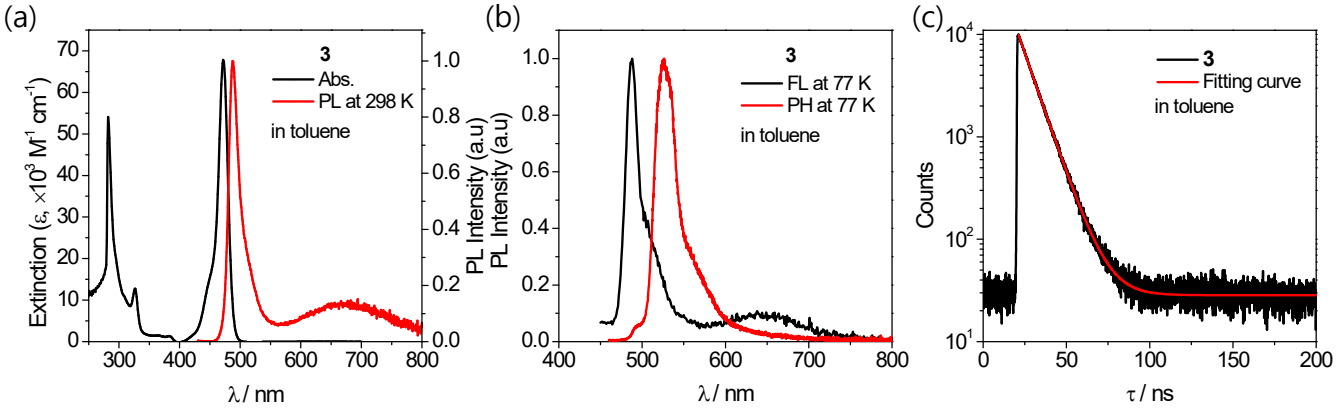

Fig. S13. (a) UV/Vis absorption and PL spectra at 298 K, (b) fluorescence and phosphorescence spectra at 77 K, and (c) transient PL decay of **3** at 298 K (2.0×10^{-5} M in toluene).

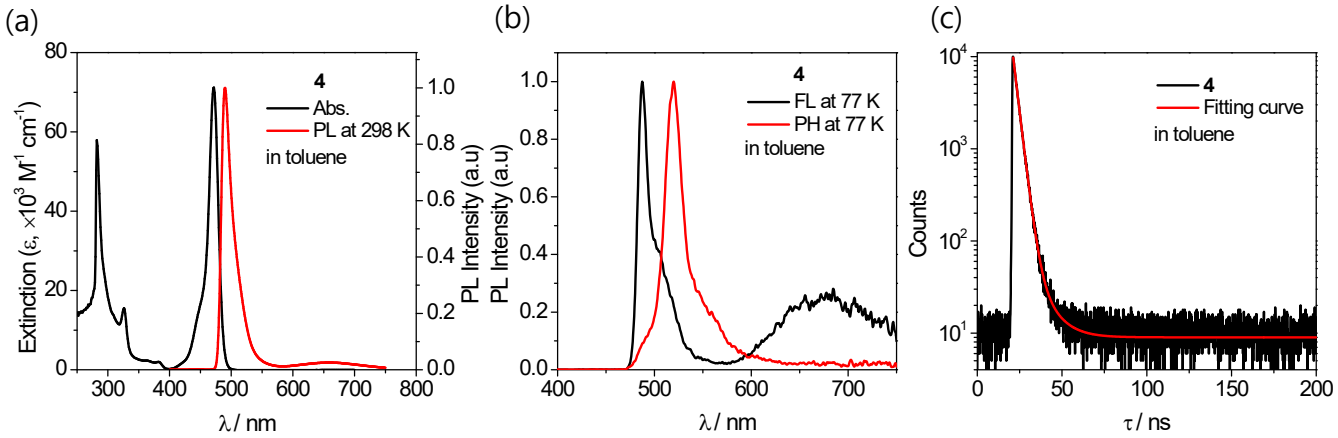

Fig. S14. (a) UV/Vis absorption and PL spectra at 298 K, (b) fluorescence and phosphorescence spectra at 77 K, and (c) transient PL decay of **4** at 298 K (2.0×10^{-5} M in toluene).

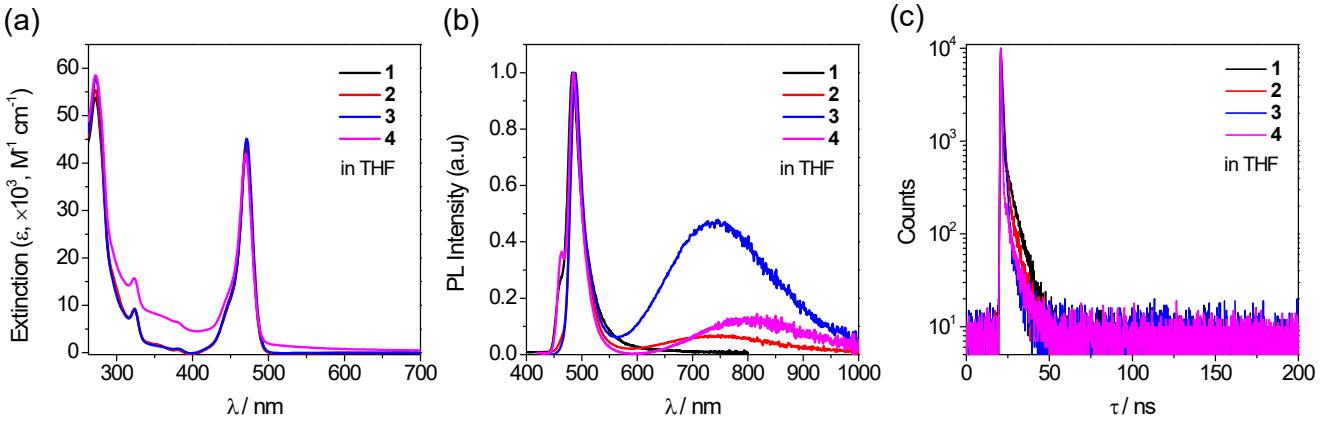

Fig. S15. (a) UV/Vis absorption, (b) PL spectra, (c) transient PL decay curves of **1**–**4** at 298 K (2.0×10^{-5} M in THF).

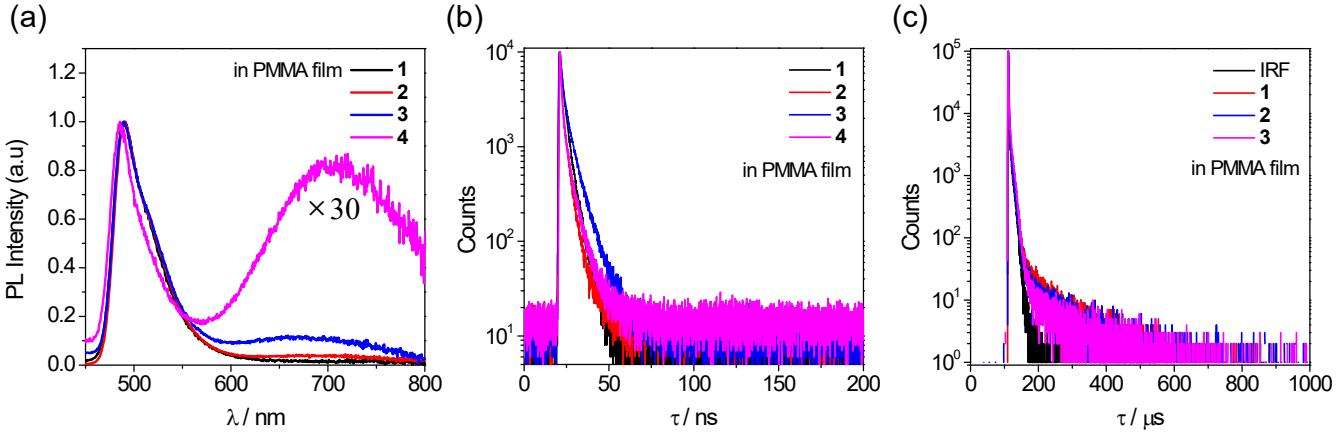

Fig. S16. (a) PL spectra and (b) prompt and (c) delayed PL decay curves of the PMMA films doped with 5 wt% of **1**–**4** at 298 K. Due to its low emission intensity, the delayed PL decay curve of **4** could not be acquired.

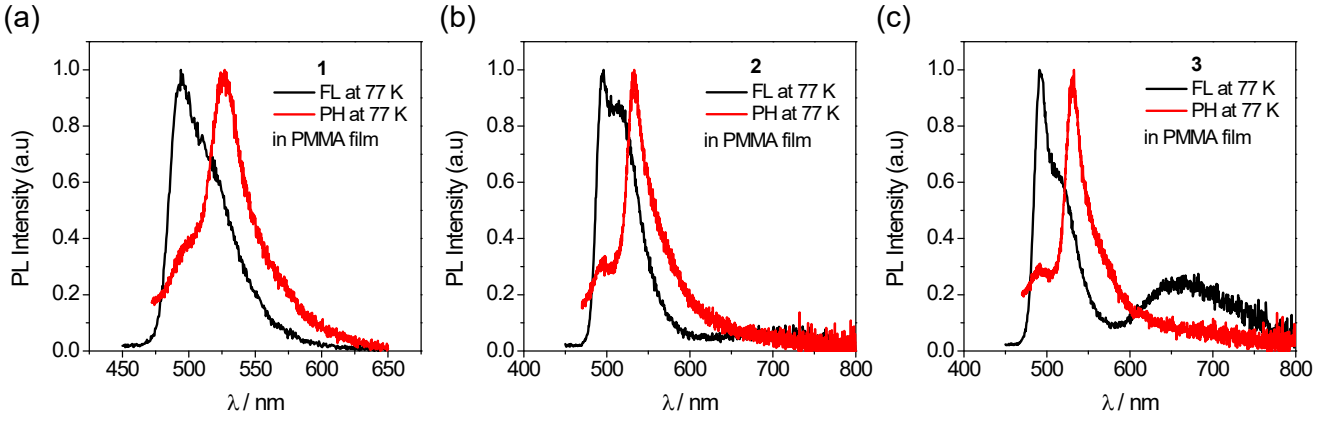

Fig. S17. Fluorescence and phosphorescence spectra of the PMMA films doped with 5 wt% of (a) **1**, (b) **2**, and (c) **3** at 77 K.

Computational details

Table S1. The C_{CB}–C_{CB} bond lengths (d(C_{CB}–C_{CB})) and their dihedral angles (ψ) with respect to the molecular plane of MR core for the S_0, S_1, T_1, and T_2-state geometries of **1**, **2**, and **4**, which were optimized at the PBE0/def2-SVP level of theory with SCRF approximation (solvent = toluene).

	1		**2**		**4**	
	d(C_{CB}–C_{CB}) (Å)	ψ (°)	d(C_{CB}–C_{CB}) (Å)	ψ (°)	d(C_{CB}–C_{CB}) (Å)	ψ (°)
S_0	1.65	89.65	1.68	90.23	1.68	81.30
S_1	1.67	89.06	1.73	90.72	1.71	83.84
T_1	1.68	90.01	1.75	91.50	1.72	86.35
T_2	1.65	72.07	1.69	93.63	1.68	80.97

Table S2. Molecular orbital distributions (in %) of **1**–**4** at their ground state (S_0) optimized geometries in toluene.

Compound	MO	MR core	CB	R
1	HOMO	99.44	0.56	0.00
	LUMO	95.17	4.79	0.04
2	HOMO	99.41	0.58	0.01
	LUMO	93.22	6.60	0.18
3	HOMO	99.36	0.57	0.07
	LUMO	93.70	6.14	0.15
4	HOMO	99.27	0.52	0.22
	LUMO	94.83	4.95	0.22

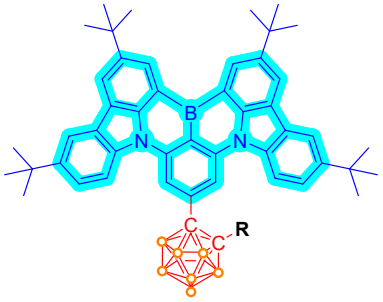

Blue: MR core

Red: *o*-carborane (CB)

(a) DtBuCzB-CBH (**1**)

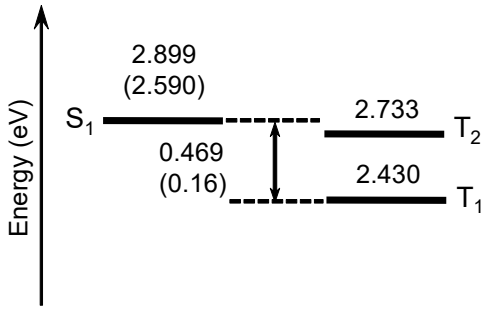

$\langle S_1|\hat{H}_{SOC}|T_2\rangle = 0.069\ cm^{-1}$
$\langle S_1|\hat{H}_{SOC}|T_1\rangle = 0.013\ cm^{-1}$

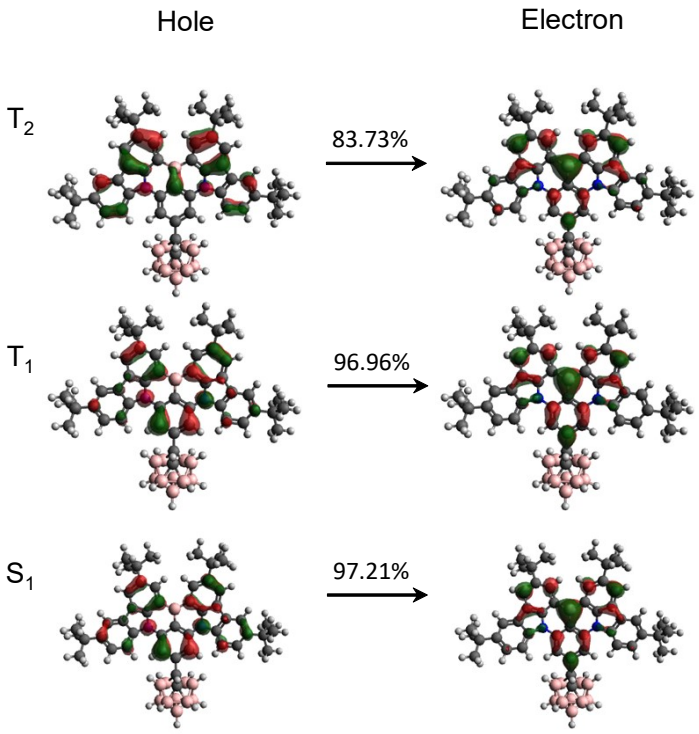

(b) DtBuCzB-CBMe (**2**)

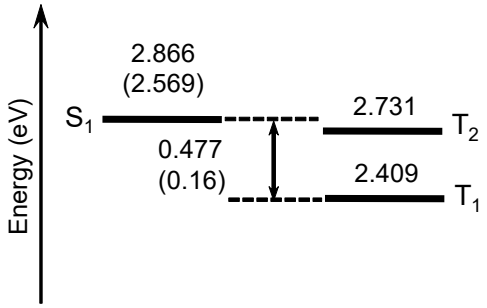

$\langle S_1|\hat{H}_{SOC}|T_2\rangle = 0.073\ cm^{-1}$
$\langle S_1|\hat{H}_{SOC}|T_1\rangle = 0.013\ cm^{-1}$

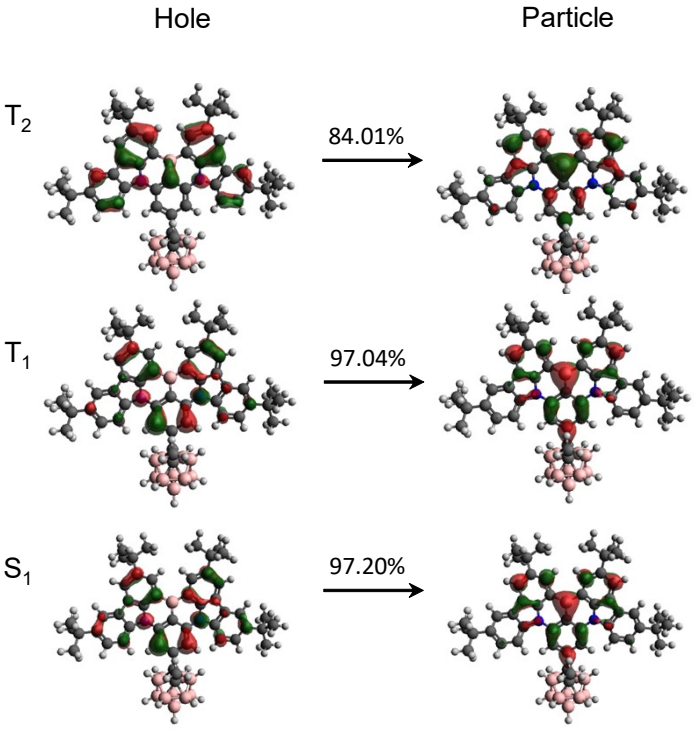

(c) DtBuCzB-CB^{i}Bu (**3**)

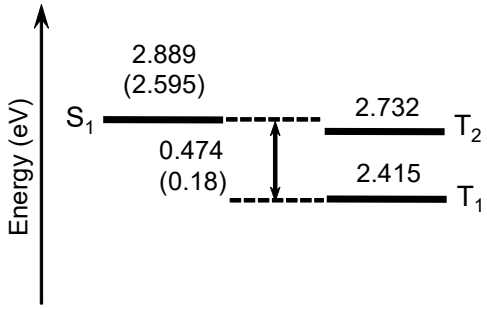

$\langle S_1|\hat{H}_{SOC}|T_2\rangle = 0.108\ cm^{-1}$
$\langle S_1|\hat{H}_{SOC}|T_1\rangle = 0.013\ cm^{-1}$

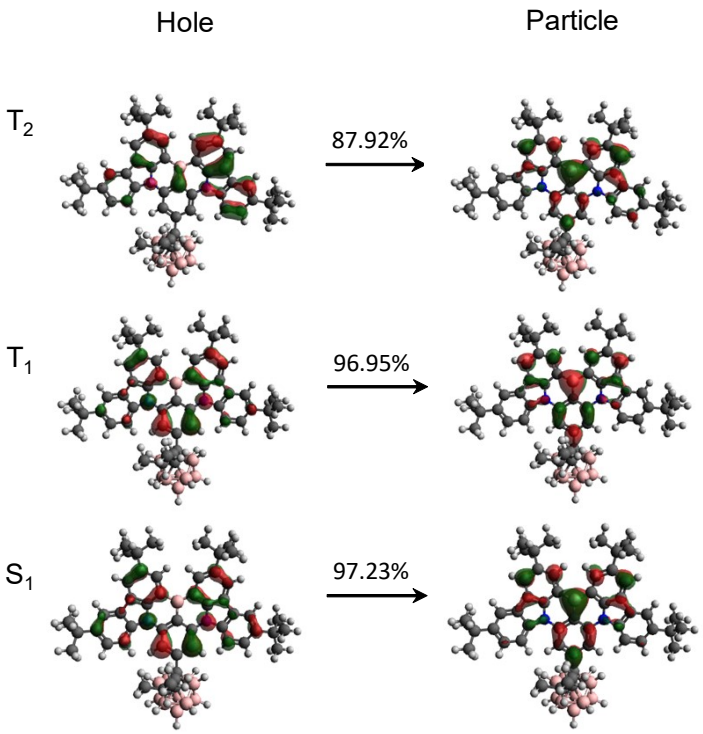

(d) DtBuCzB-CBTMS (**4**)

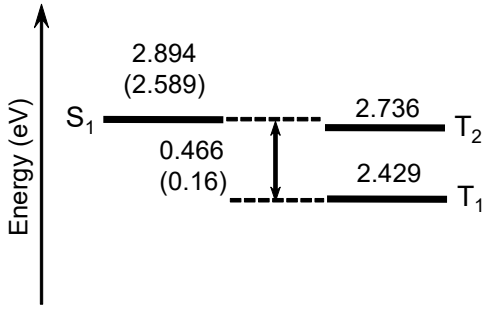

$\langle S_1|\hat{H}_{SOC}|T_2\rangle = 0.072\ cm^{-1}$
$\langle S_1|\hat{H}_{SOC}|T_1\rangle = 0.013\ cm^{-1}$

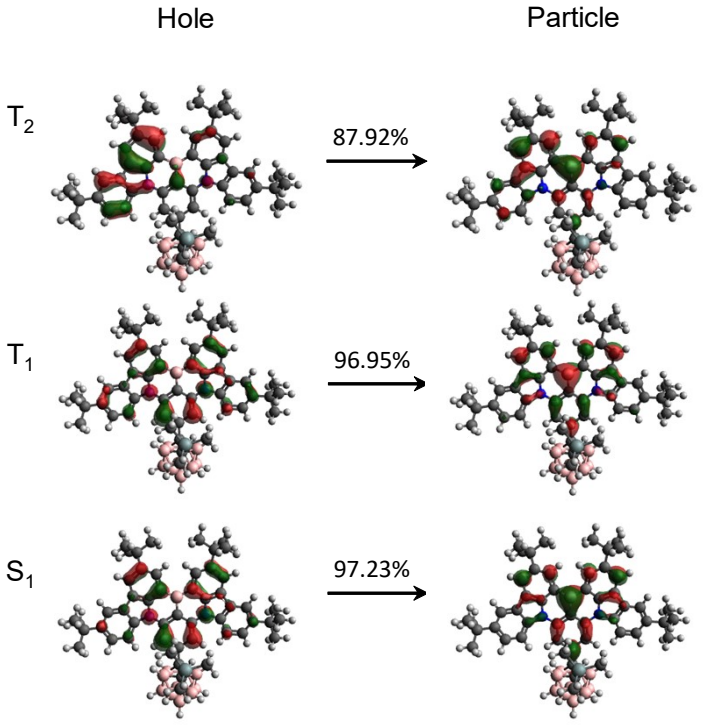

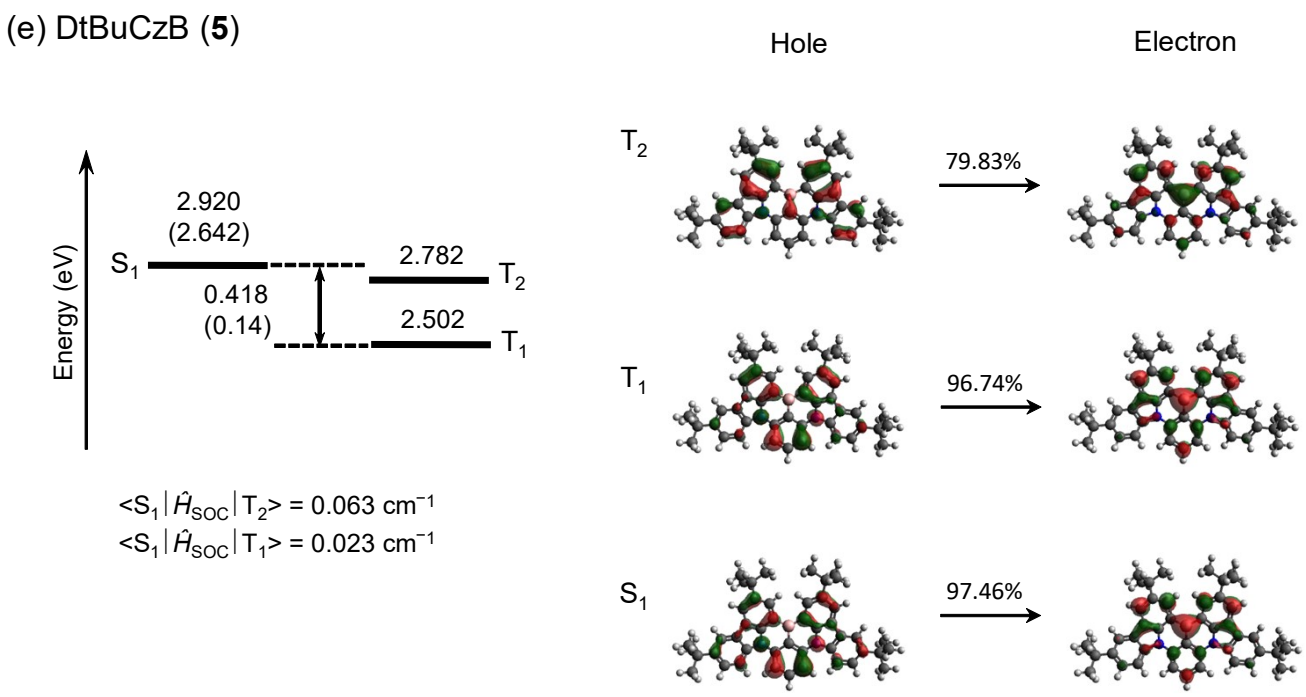

Fig. S18. Natural transition orbitals (NTOs, isovalue = 0.03 e/Å^3) of DtBuCzB-CBR (**1**−**4**) and DtBuCzB (**5**) for the transitions from S_0 to S_1, T_1, and T_2 states. Alongside the experimentally measured ΔE_{ST} values, the corrected S_1 energies are presented in parentheses since TDDFT calculation is known to overestimate ΔE_{ST} for MR-TADF molecules due to an inaccurate estimation of the Coulomb interaction mainly for S_1 state.[15,16] Additionally, the computed spin-orbit coupling (SOC) matrix elements between the S_1 and T_n (n = 1 and 2) states are provided.

Table S3. The bond lengths of C_{CB}–C_{CB}, $d(C_{CB}–C_{CB})$, and its dihedral angles (ψ) with respect to the molecular plane of MR-core for the local minimum S_1 states of **1**, **2**, and **4**. Geometry optimizations were performed with SCRF approximation (solvent = Toluene). The corresponding geometric parameters for S_0 states are presented for the comparison. The oscillator strengths (f) of local minimum S_1 states and the relative energies (in eV) of S_1-HLCT and S_1-ICT with respect to the ground state are also provided. Note that S_1-SRCT (in toluene medium) is identical to the S_1 states of **1**, **2** and **4** in **Table S1**.

		S_0	S_1-SRCT	S_1-HLCT	S_1-ICT	$\Delta E_{HLCT-ICT}$
1	$d(C_{CB}–C_{CB})$ (Å)	1.65	1.67	2.37	2.42	
	ψ (°)	89.65	89.06	89.16	7.92	
	Oscillator strength (f)	-	0.6899	0.0422	0.0007	
	Energy (eV)		2.8990	2.5373	2.5402	0.0029
2	$d(C_{CB}–C_{CB})$ (Å)	1.68	1.73	2.37	2.43	
	ψ (°)	90.23	90.72	90.18	23.96	
	Oscillator strength (f)	-	0.6860	0.0620	0.0082	
	Energy (eV)		2.8858	2.5765	2.6609	0.0844
4	$d(C_{CB}–C_{CB})$ (Å)	1.68	1.71	2.39	2.40	
	ψ (°)	81.30	83.84	89.64	31.55	
	Oscillator strength (f)	-	0.6705	0.0421	0.0076	
	Energy (eV)		2.8944	2.4310	2.6338	0.2028

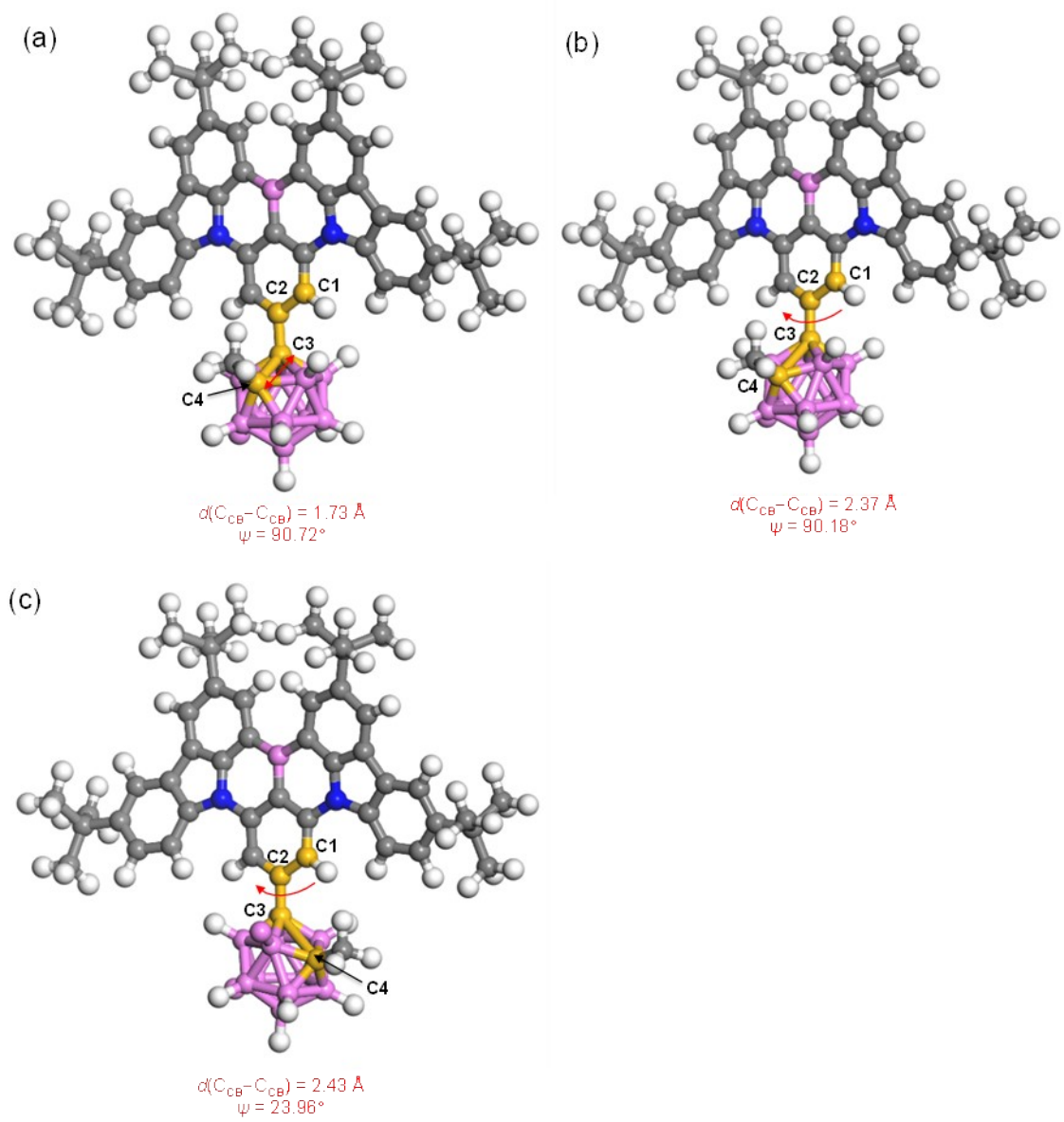

Fig. S19. Optimized geometries of (a) **2**-S_1-SRCT, (b) **2**-S_1-HLCT, and (c) **2**-S_1-ICT states in toluene medium. The bond length between C3 and C4 corresponds to $d(C_{CB}–C_{CB})$ and the dihedral angle (ψ) is defined with four atoms from C1 to C4 (yellow-colored). The direction of $C_{CB}–C_{CB}$ bond elongation is indicated with the red arrow in (a), while the dihedral rotation is indicated with the curved red arrow in (b) and (c). Potential energy surface (PES) upon $C_{CB}–C_{CB}$ bond elongation was constructed by increasing the bond length in approximately 0.1 Å increments, while the rotational PES was constructed by increasing the dihedral angle (ψ) from 90° to 0°, with 10° increments. Similar treatments were done for **1** and **4** at their S_1-SRCT, S_1-HLCT, S_1-ICT states, respectively.

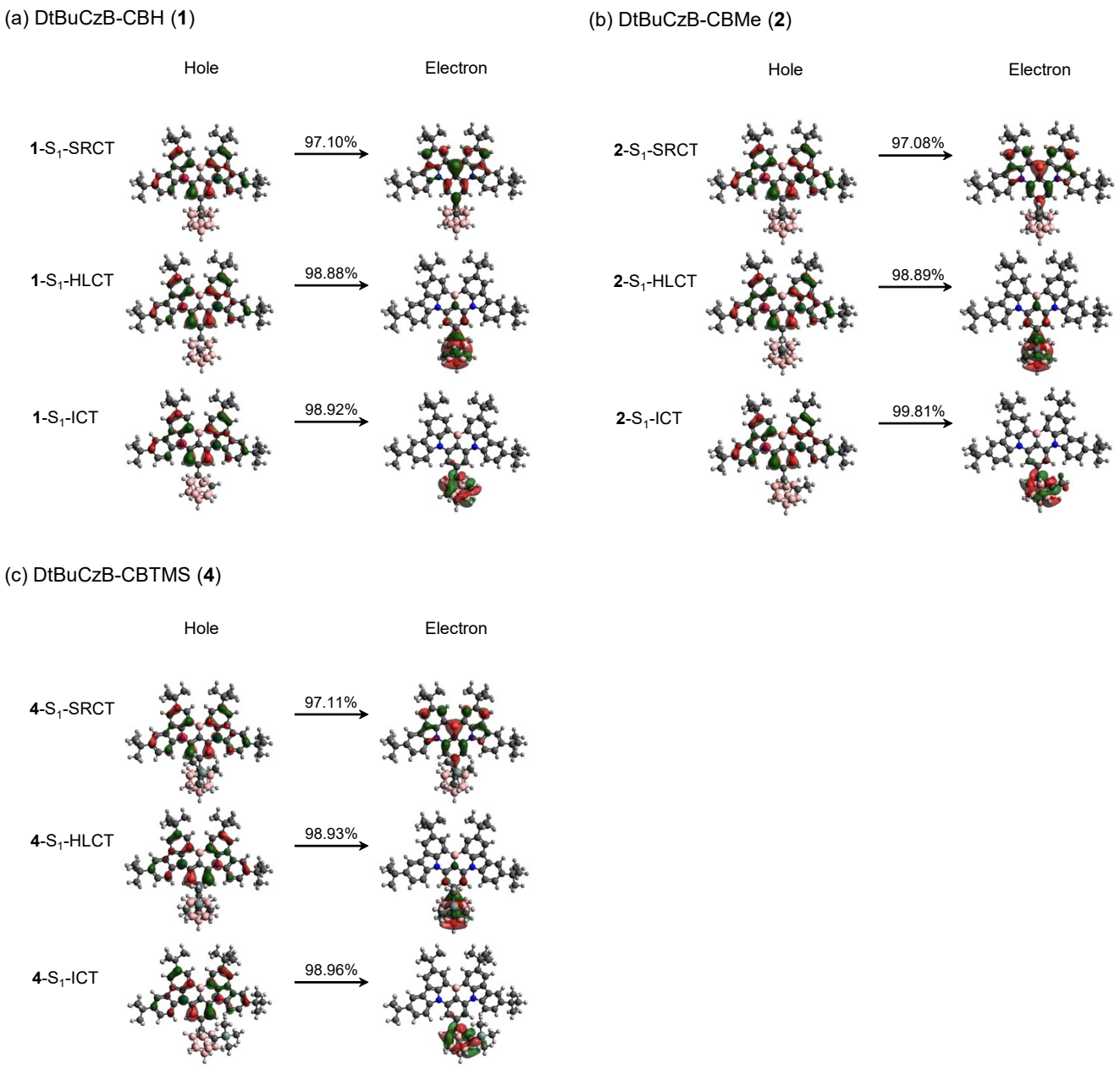

Fig. S20. NTOs (isovalue = 0.03 e/Å^3) of the local minimum excited states of **1**, **2**, and **4**.

Table S4. Hole and electron NTO distributions (in %) for the S_1-HLCT and S_1-ICT states of compounds **1**, **2**, and **4** at their excited (S_1) optimized local minima geometries in toluene.

State	MO	MR core	CB	R
1-S_1-HLCT	Hole	99.45	0.55	0.00
	Electron	15.49	83.95	0.56
1-S_1-ICT	Hole	99.44	0.55	0.01
	Electron	2.74	96.55	0.71
2-S_1-HLCT	Hole	99.49	0.51	0.00
	Electron	18.30	79.01	2.69
2-S_1-ICT	Hole	99.50	0.44	0.06
	Electron	4.81	92.06	3.12
4-S_1-HLCT	Hole	99.34	0.51	0.15
	Electron	14.89	82.15	2.96
4-S_1-ICT	Hole	99.41	0.49	0.10
	Electron	3.99	92.22	3.79

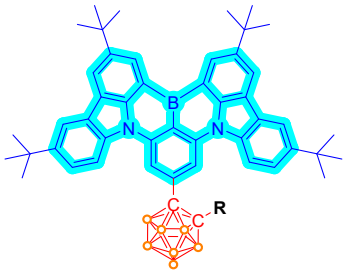

Blue: MR core

Red: *o*-carborane (CB)

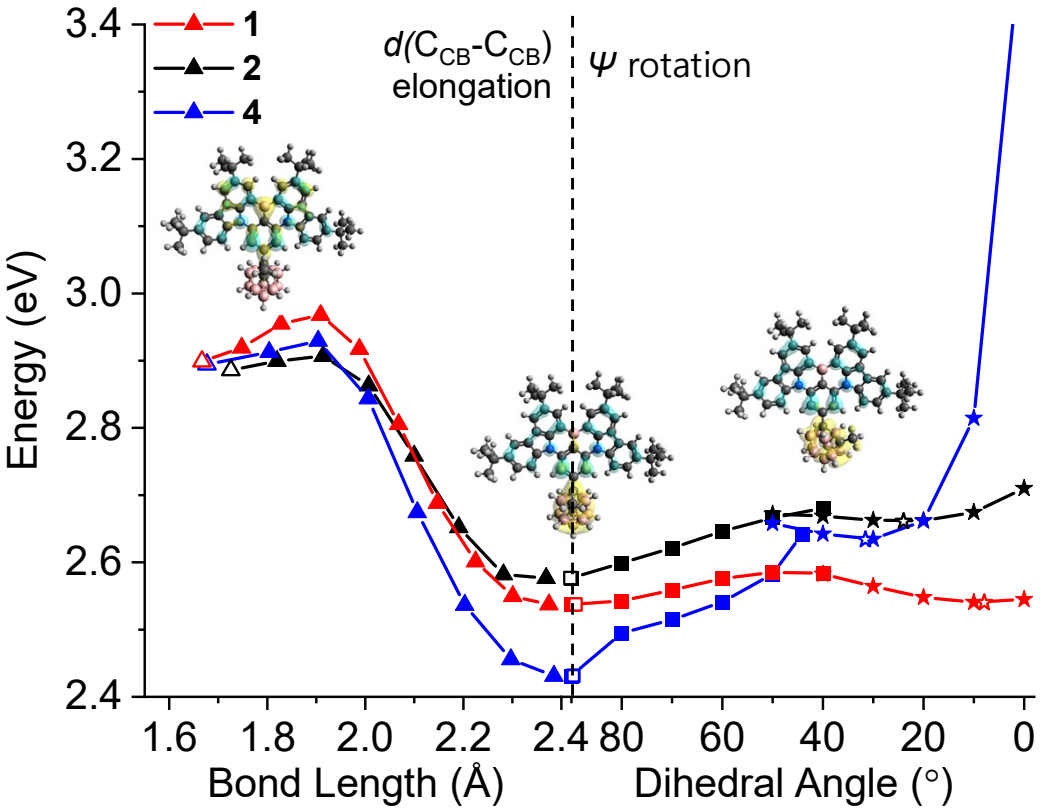

Fig. S21. Potential energy surfaces (PES) with respect to reaction coordinates from the bright S_1-SRCT to the dark S_1-ICT states through the bright S_1-HLCT state for compounds **1** (red line), **2** (black line), and **4** (blue line). The left and right sides of PES correspond to energy variations via elongation of $d(C_{CB}–C_{CB})$ and the dihedral rotation (ψ), respectively (see **Fig. S21–S22** for the details of PES construction). The NTO of each state are visualized with cyan for hole orbitals and with yellow for electron orbitals (isovalue = 0.03 e/Å^3). Empty symbols denote the optimized geometries in their local minimum excited states.

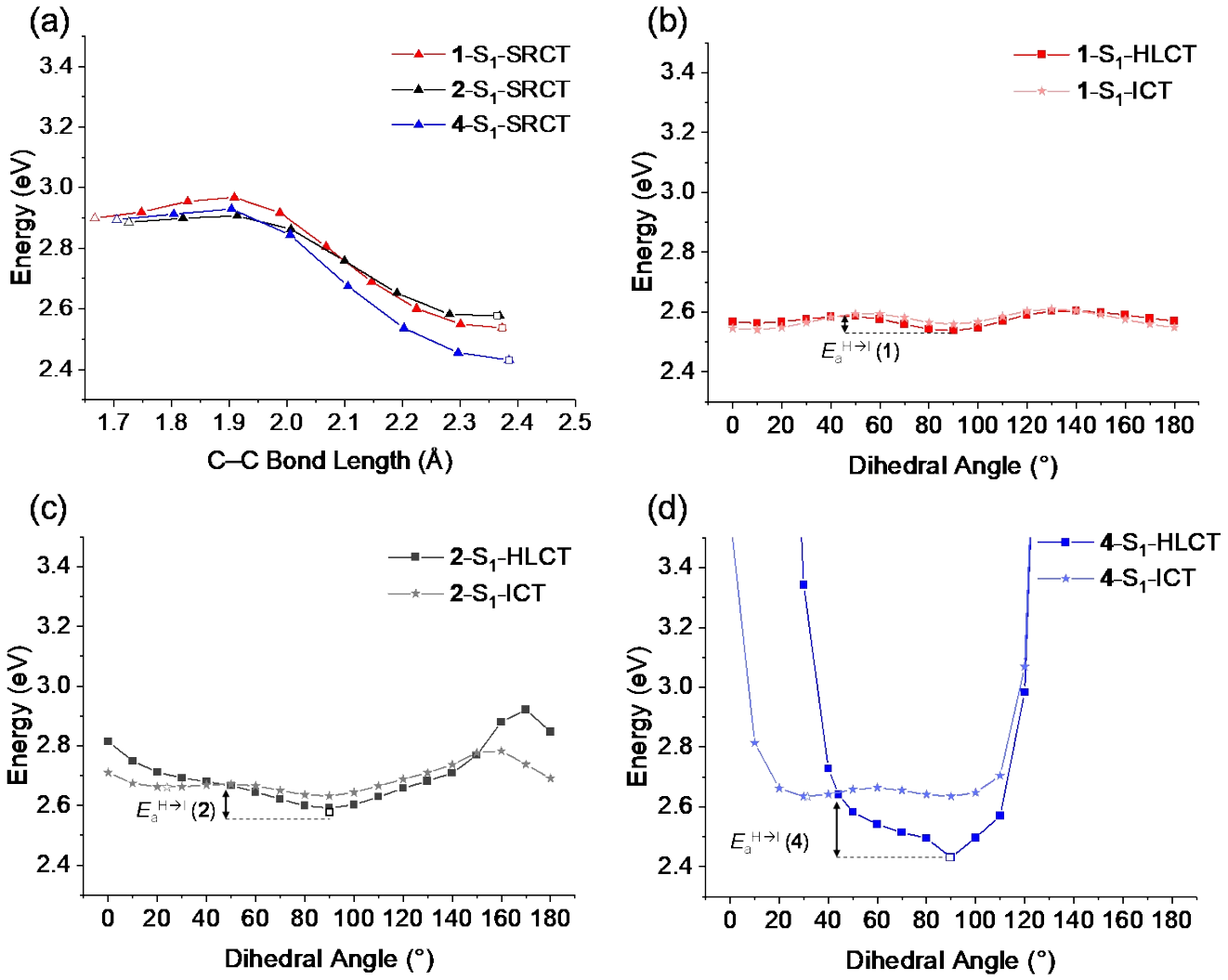

Fig. S22. (a) PES of **1**-S_1-SRCT, **2**-S_1-SRCT, and **4**-S_1-SRCT states generated by elongating the C_{CB}–C_{CB} bond incrementally at fixed dihedral angle (ψ) until S_1-HLCT is reached. (b) PES of **1**-S_1-HLCT and **1**-S_1-ICT with varying ψ. (c) PES of **2**-S_1-HLCT and **2**-S_1-ICT with varying ψ. (d) PES of **4**-S_1-HLCT and **4**-S_1-ICT with varying ψ. The activation energies ($E_a^{H\rightarrow I}$) were calculated from the difference between the energy at the optimized HLCT state and the crossover point to the PES of ICT state. Empty shapes denote the optimized structure of each state.

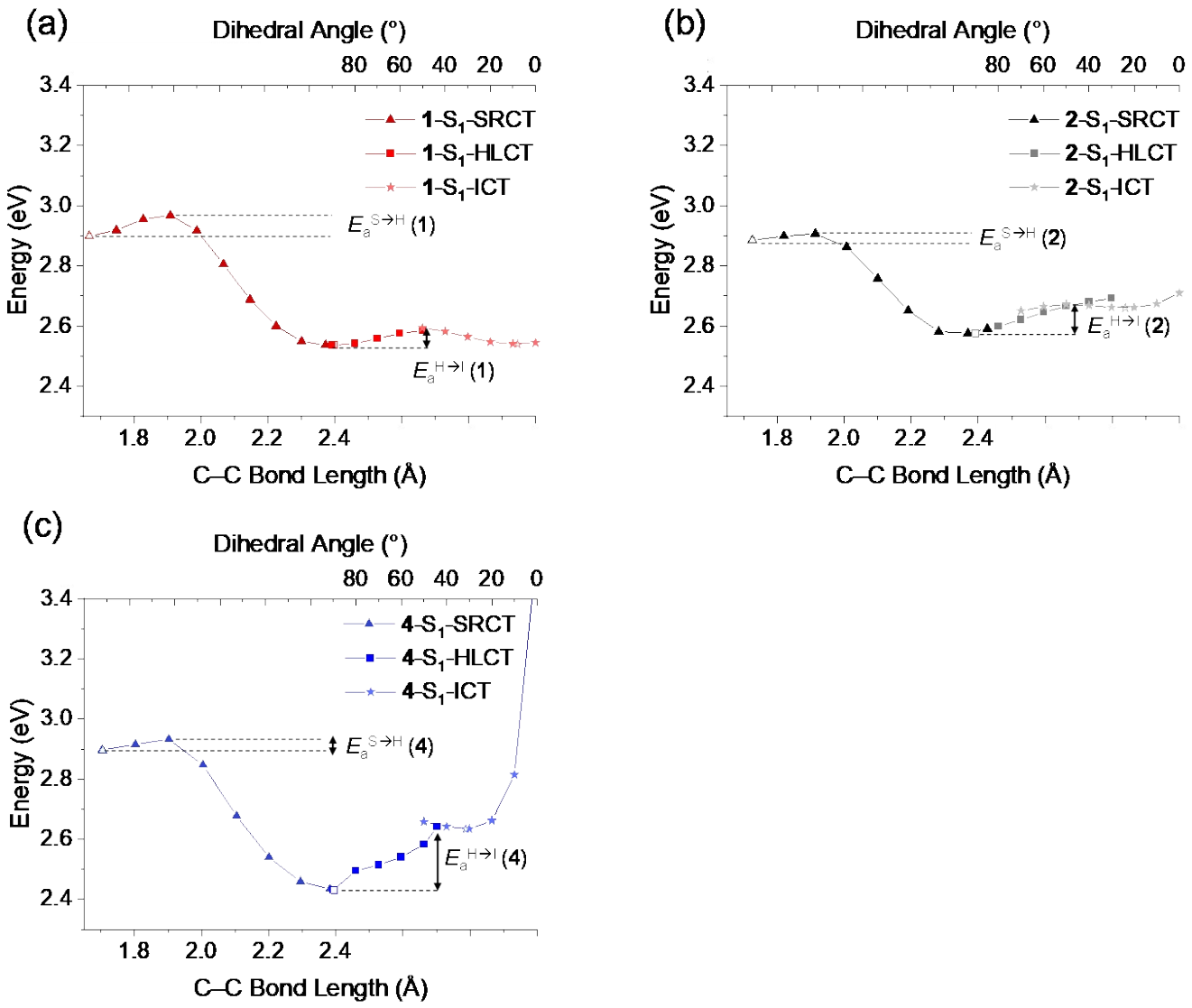

Fig. S23. Combined PES for (a) **1**, (b) **2**, and (c) **4**. The reaction coordinate was generated by combining the PES of all three states by elongating $d(C_{CB}–C_{CB})$ at fixed dihedral angle, followed by rotating ψ.

Table S5. The C_{CB}–C_{CB} bond lengths (d(C_{CB}–C_{CB})) and their dihedral angles (ψ) with respect to the molecular plane of MR-core for the local minimum S_1 states of **1**, **2**, and **4**. Geometry optimizations were performed with SCRF approximation (solvent = THF). The corresponding geometric parameters for the S_0 state are presented for comparison. The oscillator strengths (f) of local minimum S_1 states and the relative energies (in eV) of S_1-HLCT and S_1-ICT with respect to the ground state are also provided.

		S_0	S_1-SRCT	S_1-HLCT	S_1-ICT	$\Delta E_{HLCT-ICT}$
1	d(C_{CB}–C_{CB}) (Å)	1.64	1.67	2.37	2.42	
	ψ (°)	83.71	85.51	89.38	7.77	
	Oscillator Strength (f)	-	0.8014	0.0536	0.0008	
	Energy (eV)		2.8445	2.5276	2.5600	0.0324
2	d(C_{CB}–C_{CB}) (Å)	1.68	1.73	2.36	2.44	
	ψ (°)	91.00	90.19	89.73	12.29	
	Oscillator Strength (f)	-	0.7953	0.0792	0.0057	
	Energy (eV)		2.8305	2.5679	2.6987	0.1308
4	d(C_{CB}–C_{CB}) (Å)	1.68	1.71	2.39	2.40	
	ψ (°)	82.11	84.14	90.04	20.01	
	Oscillator Strength (f)	-	0.7862	0.0530	0.0042	
	Energy (eV)		2.8404	2.4054	2.6639	0.2585

References

1. X. Xiao, B. Lei, D. Wu and Z. Bin, "Medium-Ring" Strategy Enables High-Performance Narrowband Pure-Blue Multi-Resonance Emitters: Boost Provided by a Unique Perpendicular Geometry**,** *Chem. Commun*. 2023, **59**, 6556−6559.
2. Y. Xu, Z. Cheng, Z. Li, B. Liang, J. Wang, J. Wei, Z. Zhang and Y. Wang, Molecular-Structure and Device-Configuration Optimizations toward Highly Efficient Green Electroluminescence with Narrowband Emission and High Color Purity, *Adv. Optical Mater*. 2020, **8**, 1902142.
3. G. Sheldrick, Crystal Structure Refinement with *SHELXL*, *Acta Cryst. C* 2015, **71**, 3−8.
4. O. V. Dolomanov, L. J. Bourhis, R. J. Gildea, J. A. K. Howard and H. Puschmann, *OLEX2*: a Complete Structure Solution, Refinement and Analysis Program, *J. Appl. Crystallogr.* 2009, **42**, 339−341.
5. S. Hirata and M. Head-Gordon, Time-Dependent Density Functional Theory within the Tamm-Dancoff Approximation, *Chem. Phys. Lett.* 1999, **314**, 291−299.
6. C. Adamo and V. Barone, Toward Reliable Density Functional Methods without Adjustable Parameters: The PBE0 Model, *J. Chem. Phys.* 1999, **110**, 6158−6170.
7. F. Weigend and R. Ahlrichs, Balanced Basis Sets of Split Valance, Triple Zeta Valance and Quadruple Zeta Valance Quality for H to Rn: Design and Assessment of Accuracy, *Phys. Chem. Chem. Phys.* 2005, **7**, 3297−3305.
8. M. J. Frisch, G. W. Trucks, H. B. Schlegel, G. E. Scuseria, M. A. Robb, J. R. Cheeseman, G. Scalmani, V. Barone, G. A. Petersson, H. Nakatsuji, X. Li, M. Caricato, A. V. Marenich, J. Bloino, B. G. Janesko, R. Gomperts, B.; Mennucci, H. P. Hratchian, J. V. Ortiz, A. F. Izmaylov, J. L. Sonnenberg, D. Williams-Young, F.; Ding, F. Lipparini, F. Egidi, J. Goings, B. Peng, A.Petrone, T. Henderson, D. Ranasinghe, V. G. Zakrzewski, J. Gao, N. Rega, G. Zheng, W. Liang, M. Hada, M. Ehara, K. Toyota, R. Fukuda, J. Hasegawa, M. Ishida, T. Nakajima, Y. Honda, O. Kitao, H. Nakai, T. Vreven, K. Throssell, J. A. Montgomery, J. E. Jr.; Peralta, F. Ogliaro, M. J. Bearpark, J. J Heyd, E. N. Brothers, K. N. Kudin, V. N. Staroverov, T. A. Keith, R. Kobayashi, J. Normand, K. Raghavachari, A. P. Rendell, J. C. Burant, S. S. Iyengar, J. Tomasi, M. Cossi, J. M. Millam, M. Klene, C. Adamo, R. Cammi, J. W. Ochterski, R. L. Martin, K. Morokuma, O. Farkas, J. B. Foresman and D. J. Fox, Gaussian 16, Revision C.01, Gaussian, Inc., Wallingford CT, 2019.
9. J. Tomasi, B. Mennucci and R. Cammi, Quantum Mechanical Continuum Solvation Models, *Chem. Rev.* 2005, **105**, 2999−3093.
10. R. L. Martin, Natural Transition Orbitals, *J. Chem. Phys.* 2003, **118**, 4775−4777.
11. T. Lu and F. Chen, Multiwfn: a Multifunctional Wavefunction Analyzer, *J. Comput. Chem*. 2012, **33**, 580−592.

12. S. I. Gorelsky and A. B. P. Lever, Electronic Structure and Spectra of Ruthenium Diimine Complexes by Density Functional Theory and INDO/S. Comparison of the Two Methods, *J. Organomet. Chem.* 2001, **635**, 187−196.

13. B. de Souza, G. Farias, F. Neese and R. Izsak, Predicting Phosphorescence Rates of Light Organic Molecules Using Time-Dependent Density Functional Theory and the Path Integral Approach to Dynamics, *J. Chem. Theory Comput.* 2019, **15**, 1896−1904.

14. F. Neese, The ORCA Program System, *WIREs Comput. Mol. Sci*. 2011, **2**, 73−78; F. Neese, Software Update: the ORCA Program System, Version 4.0, *WIREs Comput. Mol. Sci*. 2018, **8**, e1327.

15. K. Shizu, H. Kaji, Comprehensive Understanding of Multiple Resonance Thermally Activated Delayed Fluorescence Through Quantum Chemistry Calculation, *Commun. Chem.* 2022, **5**, 53.

16. A. Pershin, D. Hall, V. Lemaur, J. C. Sancho-Garcia, L. Muccioli, E. Zysman-Colman, D. Beljonne, Y. Olivier, Highly Emissive Excitons with Reduced Exchange Energy in Thermally Activated Fluorescent Molecules, *Nat. Commun.* 2019, **10**, 597.